Centre for Geo-Information

Thesis Report GIRS-2014-27

Performance of the Enhanced Vegetation Index to Detect Inner-annual Dry Season and Drought Impacts on Amazon Forest Canopies

Benjamin Brede

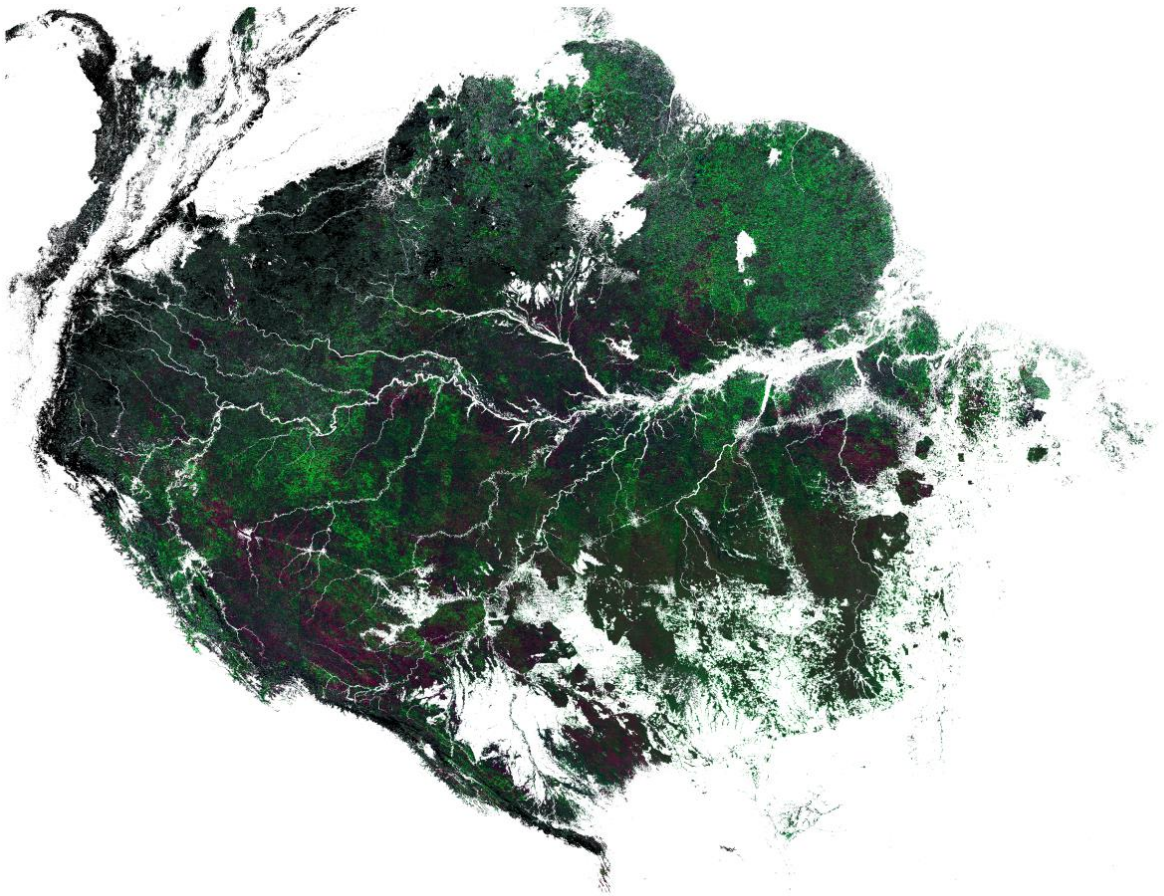

July 2014

WAGENINGEN UNIVERSITY
WAGENINGEN UR

Performance of the Enhanced Vegetation Index to Detect Inner-annual Dry Season and Drought Impacts on Amazon Forest Canopies

Benjamin Brede

Registration number 88 03 11 120 130

Supervisors:

Dr. Jan Verbesselt

Loïc P. Dutrieux, M.Sc.

A thesis submitted in partial fulfilment of the degree of Master of Science
at Wageningen University and Research Centre,
The Netherlands.

July 2, 2014

Wageningen, The Netherlands

Thesis code number: GRS-80436
Thesis Report: GIRS-2012-27
Wageningen University and Research Centre
Laboratory of Geo-Information Science and Remote Sensing

Acknowledgements

First of all, I would like to thank my supervisors Jan Verbesselt and Loïc Dutrieux for guiding this research and leaving me the freedom to explore data and ideas. Further thanks go to Jan Clevers for valuable discussions about BRDF modelling. This helped me to see the modelling process with more critical eyes. I also thank Bart Kruijt for sharing his first-hand knowledge of the Amazon tropical forests and for discussions in the early stages of this research. It saved me from running miles into a wrong direction.

Further thanks go to the Fluxnet community for their efforts in compiling the LaThuile data set. The tropical forests challenge people and equipment with a totally different quality compared to what I experience in my comfortable office chair. But large, harmonised data sets are needed to answer fundamental questions.

Another gratitude goes to the open source community, or better several communities for providing great software tools: the R environment, RStudio, LaTeX, LyX, GDAL, to name only some. Nowadays, freely accessible tools make it possible for everyone to solve complex problems without spending years on developing the appropriate software.

I would also like to thank my family for their unconstrained support during my studies. And finally Anna for reminding me that eating and sleeping are not habits of luxury.

Abstract

The Amazon rainforests represent the largest connected forested area in the tropics and play an integral role in the global carbon cycle. In the last years the discussion about their phenology and response to drought has become intense. A recent study argues that greenness seasonality expressed as Enhanced Vegetation Index (EVI) is an artifact of variations in sun-sensor geometry throughout the year. In this study I aimed to reproduce these results with the Moderate-Resolution Imaging Spectroradiometer (MODIS) MCD43 product suite. With this data set modelling of reflectances at fixed sun and viewing geometry was possible. The derived EVI was spatially aggregated over large areas of central Amazon forests. The resulting time series of EVI contained distinct seasonal patterns, but was also correlated with the sun geometry expressed as Solar Zenith Angle (SZA). Second, I conducted a validation approach to test the performance of EVI for predicting canopy carbon uptake and structural changes. This involved field data from eddy covariance towers and forest phenology plots. I used the Vegetation Photosynthesis Model (VPM) – a carbon uptake model – to translate EVI into estimates for Gross Primary Productivity (GPP). Besides, I directly compared EVI dynamics with canopy leaf flush time series. In both cases EVI showed low predictive power for the ground processes, but was again correlated with SZA. Third, I assessed EVI's sensitivity to drought. For that I analysed the relationship between Bidirectional Reflectance Distribution Function (BRDF)-adjusted EVI dry season anomalies and two drought indices. This analysis covered whole Amazonia and data from the years 2000 to 2013. The drought indices were derived from the Tropical Rainfall Measuring Mission Multisatellite Precipitation Analysis (TMPA) 3B42 V7 precipitation product. The results contained no general, meaningful connection between EVI anomalies and drought indices. Despite shortcomings in the individual assessment methods, the correlation of the BRDF-adjusted EVI with the SZA is suspicious. It enforces the question if the MCD43 product can properly account for variations in Sun-Sensor Geometry Effectss (SSGEs). These results question the reliability of EVI in assessments of tropical forest canopy processes. Based on the presented results, an evaluation of the EVI's strength for ecological applications seems reasonable. This should incorporate rigorous validation supported by ground plots.

Keywords: Amazon rainforests, Moderate-Resolution Imaging Spectroradiometer, Bidirectional Reflectance Distribution Function, Enhanced Vegetation Index, dry season leaf flush, drought

Contents

List of Figures

List of Tables

1 Introduction

The Amazon rainforests represent the largest connected forested area in the tropics. They play an integral role in the global carbon cycle and store ~93±23 Pg C in above-ground living biomass alone (Malhi et al., 2006). In recent years the discussion about their resilience against transition to other stable ecosystem states has become more intense. Climate change and deforestation put pressure on the forests (Malhi et al., 2008) and the question appeared if they may partly, but abruptly transform into savannahs (White et al., 1999; Cox et al., 2004; Hirota et al., 2010).

Changing precipitation dynamics would be the main trigger for this development since they are one of the main drivers for tropical forest functioning. However, even though some General Circulation Models (GCMs) suggest a decline in dry season rainfall of up to 20% over southern and eastern Amazonia for the 21st century (Malhi et al., 2008), there is no general agreement on a future trend for the whole of Amazonia (Li et al., 2006; Christensen et al., 2007, 2013). The main reason for these uncertainties are feedbacks between the climate background state and the El Niño Southern Oscillation (ENSO). Although single processes which influence ENSO became better understood in recent years, the final ENSO variability is unclear since it is a delicate balance of all its influences (Collins et al., 2010).

The interaction between rainforests and climate introduces another uncertainty for modeling future Amazon forests. About 25 to 35% of Amazonian precipitation is recycled (Eltahir and Bras, 1994), i. e. evapotranspiration contributes significantly to rainfall. The gross vegetation cover needs to be sustained to uphold this mechanism. Deforestation or non-linear responses of vegetation to negative trends in precipitation may lead to a break down of this feedback cycle. For instance, Cox et al. (2004) observed this positive feedback between declining precipitation and shrinking forests in a coupled climate-vegetation model. It resulted in dying Amazon forests.

However, not all GCMs coupled with vegetation models show Amazon forest die-back (Marengo et al., 2011). So the question arises why is this the case? Besides the response of tropical forests to an elevated atmospheric CO_2-content (Rammig et al., 2010), the impact of droughts is a major source of error (Sitch et al., 2008). With regard to possible drying trends in the Amazon basin, it may also be the most severe. If the forests are vulnerable to droughts, increasing dryness and accompanied stronger dry seasons may damage the forest, lead to forest loss and positive feedback loops as described by Cox et al. (2004).

The discussion of drought impacts has been vivid in the past years partially due to the severe droughts in 2005 and 2010 and its implications. In a fast response survey Phillips et al. (2009) assessed the impact of the 2005 drought on tree biomass in long-term forest census plots and found major biomass losses, which ended a long-term trend in tree carbon assimilation. Phillips et al. (2010) refined this analysis. They found evidence for elevated mortality rates 2 years after the meteorological event. Furthermore, large trees had a disproportionately high mortality during the drought. This is supported by de Toledo et al. (2013).

In an experimental set up Nepstad et al. (2002) excluded nearly half of the throughfall precipitation within 2 years from reaching the ground, thereby simulating drought conditions.

This thinned the canopy and reduced above-ground Net Primary Productivity (NPP) by one fourth. They suggest an impact on the long-term species composition. Brando et al. (2008) report changes on the same experiment site after 4 years of throughfall exclusion. The trend in reduced above-ground NPP continued. Additionally, they find stronger reduction in stem growth for large compared to smaller trees. Therefore, observational and experimental forest plot studies point to an altered forest structure and reduced NPP as a long term drought effect.

On the other hand, Schwalm et al. (2010) found a positive response of NPP to relative drought. Actually, some studies found higher rates of carbon uptake during the dry compared to the wet season (Saleska et al., 2003; Hutyra et al., 2007). Instead of precipitation regimes, carbon uptake was controlled by phenology and light conditions (Hutyra et al., 2007). This does not contradict the aforementioned studies. The idea would be that water shortage as it occurs regularly in dry seasons does not necessarily lead to water shortage for the trees as some have access to soil water via deep roots (Nepstad et al., 1994). However, prolonged dryness depletes the soil water storage and eventually shows effects in tree health and carbon uptake. This means that regular dry seasons may first lead to increased carbon uptake, but the effect turns when the dry season turns into drought.

Besides ground plots, satellite remote sensing delivers information about spatial and temporal patterns of drought impacts. Frolking et al. (2011) as well as Saatchi et al. (2013) used radar observations from the SeaWinds Scatterometer on board the QuickSCAT (Quick Scatterometer) satellite to investigate forest microwave backscatter between 1999 and 2009. Microwave backscatter from radar is related to canopy structure and dielectric properties, which are predominated by water content (Kasischke et al., 1997). Both studies found high anomalies over W Amazonia (4°S–12°S, 76°W–66°W) between July to October 2005, indicating strong impact of the drought on canopy structure and water content. Additionally, Saatchi et al. (2013) discovered a persisting low backscatter in W Amazonia of >4 years, which points to slow recovery rates of the forests. This is in agreement with Phillips et al. (2010). Liu et al. (2013) also detected anomalies with a passive microwave product. Passive microwave responds similarly to vegetation and canopy water content as radar measurements. Overall, studies using active and passive microwave find clear drought impacts on the forest canopy.

In the domain of optical remote sensing there has been an intense debate about interpretation of data products in recent years. The most prominent example is probably the study of Saleska et al. (2007). They used Moderate-Resolution Imaging Spectroradiometer (MODIS) Enhanced Vegetation Index (EVI) to investigate the impacts of the 2005 drought on canopy greenness. Their derived EVI for July to September 2005 showed strong positive anomalies over wide parts of central and southern Amazonia. They explained this greening with increased light availability due to decreased cloudiness, which stimulates forest growth and concluded that the forests would not suffer from the drought. This would mean that they are much more resilient than anticipated. It would also mean that ecosystem productivity in Amazon rainforests is limited by light rather than by water availability as pointed out by Nemani et al. (2003). Samanta et al. (2010) failed to reproduce the EVI anomalies. They suspected that the data of Saleska et al. was not properly filtered for bad quality pixels contaminated with clouds and aerosols, so that artificial canopy green-up would have been produced.

However, the resilience to droughts predicted by Saleska et al. (2007) contradicts studies of forest plots and microwave remote sensing. The question arises, what is the explanatory power of vegetation indices derived from optical remote sensing for rainforest functioning, especially for carbon exchange? In their review on the usage of vegetation indices, Glenn et al. (2008) call for simple applications as spatial scaling tools for phenology or primary productivity. But

especially over dense tropical canopies indices suffer from saturation as well as cloud and aerosol contamination.

In this context another topic discussed for optical remote sensing data, especially with MODIS EVI, is of importance: dry season leaf flush. This phenomenon describes the increased production of new leaves during the dry season, which happens largely independently of rainfall conditions. Deep roots allow access to soil water during this period (Nepstad et al., 1994). One possible explanation for this pattern is that the Amazon rainforests' productivity is light limited (Nemani et al., 2003) and during the dry season more radiation is available due to less cloud cover. Additionally, herbivore pressure from insects is reduced during dry seasons (Aide, 1993). For both reasons flushing leaves in that time is advantageous over leaf flush in the wet season. Although other seasonal patterns were also found in forest plot studies, there are studies that support the idea of dry season leaf flush (Anderson, 2012; Doughty and Goulden, 2008).

What makes leaf flush important for remote sensing, is its effect on the optical signal. Roberts et al. (1998) studied spectral changes over leaf life cycles in Amazon *caatinga* vegetation. Changes in the Near Infrared Reflectance (NIR) were most dominant. During the first months of leaf expansion, NIR reflectance increased, while it decreased during the last months of the leaves' lifes. Toomey et al. (2009) observed the same effect in *caatinga* and *Terra firme* forests. The reason for this change was colonization by fungi, algae and other organisms, summarized as epiphylls. This cover reduces the NIR reflectance, thereby decreasing indices like Normalized Difference Vegetation Index (NDVI) and EVI. Hence, when trees start to grow new leaves, these leaves will increase vegetation indices and the canopy "greens up".

Huete et al. (2006), Xiao et al. (2006), Myneni et al. (2007) and Samanta et al. (2012c) observed green-up over Amazonia with MODIS EVI and attributed this to canopy leaf flush. Moreover, Samanta et al. (2012c) underlines that the change in leaf optical properties is not sufficient to explain EVI variations. Also an increase in Leaf Area Index (LAI) must be part of the phenomenon. In the context of drought impacts, dry season leaf flush may complicate the analysis since additional seasonal variability is added to the time series of optical remote sensing data. Even more, leaf flush could dominate the signal, which EVI time series of Samanta et al. (2012c) suggest. On the other hand, leaf flush itself could also be affected by drought.

Recent studies raise concerns about this line of explanation for EVI seasonality over the Amazon. Silva et al. (2013) used long time series of Advanced Very High Resolution Radiometer (AVHRR) and spectral angle mapper, a method adopted from hyperspectral remote sensing, to identify 26 distinct phenoregions over the Amazon basin. With that they question the existence of uniform dry season leaf flush in all Amazon forests, but emphasize a more heterogeneous phenological landscape. Additionally, field studies did not only find increased leaf production during high radiation periods, but also synchronization with precipitation rates or river levels (Anderson, 2012).

Other studies report Sun-Sensor Geometry Effectss (SSGEs) effects of MODIS EVI. Sims et al. (2011) investigated the dependence of 3 vegetation indices on sun-sensor-geometry in 3 forest sites in the eastern US. They found that EVI was strongly influenced by view angle. They recommend that care must be taken of this effect. Galvão et al. (2011) studied MODIS and Hyperion/Earth Observing-1 (EO-1) images at different Solar Zenith Angles (SZAs). At the end of the dry season, when SZA was lowest, EVI was highest. Lower SZAs during the dry season would reduce shading within the canopy, thus increasing NIR reflectance. Since EVI is strongly correlated to NIR, it would follow this pattern over the year. Moura et al. (2012) support these findings with their study of Multi-angle Imaging SpectroRadiometer (MISR) images. MISR with its 9 separate cameras is specifically designed to study view and illumination

effects. Together, these studies underline the need to take care of sun-sensor geometry when using MODIS EVI.

Just recently, Morton et al. (2014) corrected MODIS EVI data for SSGEs. They produced monthly red and NIR reflectances and a two band EVI with reflectances normalized to constant view and solar geometry for MODIS tiles h11v09 and h12v09, which are situated over the central parts of the Amazon rainforests. Analysis of this data showed no remaining seasonal variation. They concluded that dry season green up is an artifact of changing sun-sensor-geometry throughout the year, rather than leaf flush on the ground. Additionally, the EVI correction eliminated inter-annual variability. This implicitly questions if events like droughts can be detected with MODIS EVI, especially because the 2005 drought was part of Morton et al.'s study interval.

The conclusions of Morton et al. (2014) are in conflict with previous studies. Although SSGEs have not been accounted for in other studies using MODIS EVI, forest plots suggest distinct seasonality in Amazon forest canopies' structure. Furthermore, droughts are shown to have impacts on the canopy in studies of forest plots and radar backscatter. Moreover, missing seasonality in EVI time series implicitly questions the general coupling of EVI with photosynthetic activity and canopy carbon uptake in tropical forests as assumed by ecosystem models (Xiao et al., 2005).

This study's aim was to investigate these discrepancies and to assess the performance of MODIS EVI. For that I made use of the MODIS MCD43 product suite. It allows correction for SSGEs independent from the approach of Morton et al. (2014). Based on the MCD43 data set I tested if the Amazon rainforests show seasonal dynamics in greenness expressed as EVI and especially if greenness levels are higher during the dry season. I also investigated the usability of EVI corrected for SSGEs to predict forest carbon uptake as well as the production of new leaves. Finally, I investigated the impact of drought on dry season canopy greenness. The results of this analysis need to be interpreted together: if EVI shows high predictive power for ground processes, the greenness drought sensitivity can be translated into drought sensitivity of the described ground processes. On the other hand, if the predictive power is low, the greenness concept as a proxy for canopy process is challenged.

The following research questions summarize my intentions and were leading this research:

RQ1 Do Amazon forests show seasonal (inner-annual) changes in canopy greenness with satellite remote sensing indices corrected for Sun-Sensor Geometry Effects (SSGE)?

RQ2 What is the predictive power of EVI corrected for SSGEs for canopy carbon uptake and structure?

RQ3 How is canopy greenness expressed as EVI affected by the strength of moisture stress during the dry season?

This report is structured as follows: Chapter 2 describes all data sets used. It especially emphasizes the approach to correct for SSGEs. Chapter 3 deals with the methods used to analyse the data. The study area masking strategy is described, how the vegetation indices were analysed as well as how the different data sets were combined to offer answers for the research questions. Results – mostly in the form of graphs and maps – are presented and described in Chapter 4. Possible interpretations for the results in the context of other studies and their limitations are discussed in Chapter 5. Chapter 6 offers an integrating look on all results, especially regarding possible implications of SSGEs for future studies. Also challenges that should be tackled in further studies are listed.

2 Data

This chapter gives an overview of the data sets used in this study. All of them are explicitly spatial except the ground data described in Section 2.4. A special emphasis lies on the MODIS Bidirectional Reflectance Distribution Function (BRDF) modelling process (Section 2.3), since this is the primary tool to correct for SSGEs and to account for varying SZAs throughout the year.

2.1 Landcover

I identified tropical forests with the MODIS MCD12Q1 Land Cover Type product V051. This version 051 product has – unlike its predecessor – 500 m spatial resolution (Friedl et al., 2010). and matches the resolution of the spectral data sets used (Section 2.3). It is available once a year for 2001 until 2012, which makes a total of 12 landcover observations per pixel. It contains several landcover classification schemes, of which I selected the International Geosphere-Biosphere Programme (IGBP) scheme. This scheme is commonly used in vegetation response studies of Amazonia (e.g. Xiao et al., 2006; Samanta et al., 2012c,b). The MCD12Q1 product is freely available from the MODIS data pool (https://lpdaac.usgs.gov/).

Additionally, I defined the study area as the hydrological Amazon river basin with the map of the Large-Scale Biosphere-Atmosphere Experiment in the Amazon (LBA) (Mayorga et al., 2012). The river basin map was generated by flow direction modelling based on river network data (Mayorga et al., 2005). It has 0.005° spatial resolution, which is approximately 555 m at the equator and therefore resembles the resolution of the reflectance data (Section 2.3). The data set can be accessed at http://dx.doi.org/10.3334/ORNLDAAC/1086.

2.2 Precipitation

For spatial analysis of precipitation I used the Tropical Rainfall Measuring Mission Multisatellite Precipitation Analysis (TMPA) 3B42 V7 daily accumulated precipitation product (Huffman et al., 2010). TMPA is based on data from various space-borne sensors, including passive microwave, infrared and radar, with the Tropical Rainfall Measuring Mission (TRMM) as the core satellite. The merged satellite retrievals are improved by matching monthly precipitation estimates to histograms of global rain gauge networks. The primary output are 3-hourly estimates at 0.25° spatial resolution, which are temporally aggregated to daily and monthly products. The research product version is available from January 1998 to near present from the Goddard Earth Sciences Data and Information Services Center (http://mirador.gsfc.nasa.gov/).

A wide range of studies validated TMPA precipitation data sets. Known inaccuracies are high errors at full temporal resolution, i. e. 3-hourly (Ouma et al., 2012). Users are recommended to aggregate data to their application's need and thereby reduce errors (Huffman et al., 2010). Carvalho et al. (2012) compared various gauge-based and re-analysis data sets for tropical

South America. They found good agreement between TMPA and 3 other data sets in respect to dry and wet season timing as well as mean precipitation rates at aggregated levels.

2.3 Surface reflectance

A major aim of this study was to correct spectral reflectances for SSGEs. The two MODIS sensors aboard the Aqua and Terra satellites provide unique opportunities for this purpose. Each one has a wide viewing angle, allowing a wide range of viewing geometries for pixels, and produces images under a different sun zenith angle than the other one due to the morning (Aqua) and afternoon (Terra) local overpass time. These facts allow a wide spread angular sampling, which is necessary to determine the land surface BRDF.

The MCD43 product suite contains results of fitting pixel-wise reflectance observations of 16 days to a semi-empirical, linear BRDF model, the RossThick-LiSparse-Reciprocal (RTLSR) model (Schaaf et al., 2002, 2011). This kernel based model consists of three terms, which each characterise different surface scattering processes (Lucht et al., 2000a): the isotropic parameter f_{iso} describes Lambertian reflectance, the volumetric parameter f_{vol} describes intra-crown volume scattering by leaves in the canopy and is sensitive to leaf optical properties and their spatial density, and the geometric parameter f_{geo} describes shadowing effects of canopy gaps or protrusions.

While the isotropic term is not dependent on sun and observation geometry, the volumetric and geometric terms are functions of sun and viewing geometry. Additionally, the model is inverted for each band λ separately. The Bidirectional Reflectance Factor (BRF) is modelled as a linear combination of the kernel terms:

$$BRF\left(\theta_s, \theta_v, \phi, \lambda\right) = f_{iso}\left(\lambda\right) + f_{vol}\left(\lambda\right) K_{vol}\left(\theta_s, \theta_v, \phi, \lambda\right) + f_{geo}\left(\lambda\right) K_{geo}\left(\theta_s, \theta_v, \phi, \lambda\right) \tag{2.1}$$

where BRF is the Bidirectional Reflectance Factor at view zenith angle θ_v, solar zenith angle θ_s and relative azimuth angle ϕ. The parameters f_{iso}, f_{vol} and f_{geo} represent reflectances (Roujean et al., 1992) and are scaled according to the kernel values K_{vol} and K_{geo}. The volumetric RossThick kernel K_{vol} assumes a dense leaf canopy (Roujean et al., 1992) . It models the canopy as a homogenous medium with randomly oriented facets. The kernel is written as (Strahler et al., 1999):

$$K_{vol}\left(\theta_s, \theta_v, \phi\right) = \frac{\left(\frac{\pi}{2} - \xi\right)\cos\xi + \sin\xi}{\cos\theta_s + \cos\theta_v} - \frac{\pi}{4} \tag{2.2}$$

with ξ the angle between sun and sensor, which is defined as

$$\cos\xi = \cos\theta_s \cos\theta_v + \sin\theta_s \sin\theta_v \cos\phi \tag{2.3}$$

The geometric, reciprocal LiSparse kernel K_{geo} assumes a sparse leaf canopy, i. e. non-overlapping shadows cast by randomly distributed objects. It is formulated as (Lucht et al., 2000a; Strahler et al., 1999):

$$K_{geo}\left(\theta_s, \theta_v, \phi\right) = O\left(\theta_s, \theta_v, \phi\right) - \sec\theta_s' - \sec\theta_v' + \frac{1}{2}\left(1 + \cos\xi'\right)\sec\theta_v' \sec\theta_s' \tag{2.4}$$

where

Table 2.1: Explanations for band quality levels as used in this report

Level	MCD43A2 quality description
1	best quality, full inversion (RMSE majority good)
2	good quality, full inversion
3	magnitude inversion (number of observations ≥ 7)
4	magnitude inversion (number of observations ≥ 3 & ≤ 7)

$$O\left(\theta_s, \theta_v, \phi\right) = \frac{1}{\pi}\left(t - \sin t \cos t\right)\left(\sec\theta_s^{'} + \sec\theta_v^{'}\right) \tag{2.5}$$

$$\cos t = \frac{h}{b}\frac{\sqrt{D^2 + \left(\tan\theta_s^{'}\tan\theta_v^{'}\sin\phi\right)^2}}{\sec\theta_s^{'} + \sec\theta_v^{'}} \tag{2.6}$$

$$D = \sqrt{\tan^2\theta_s^{'} + \tan^2\theta_v^{'} - 2\tan\theta_s^{'}\tan\theta_v^{'}\cos\phi} \tag{2.7}$$

$$\cos\xi^{'} = \cos\theta_s^{'}\cos\theta_v^{'} + \sin\theta_s^{'}\sin\theta_v^{'}\cos\phi \tag{2.8}$$

$$\theta_s^{'} = \tan^{-1}\left(\frac{b}{r}\tan\theta_s\right),\ \theta_v^{'} = \tan^{-1}\left(\frac{b}{r}\tan\theta_v\right) \tag{2.9}$$

For MODIS processing the dimensionless crown relative height and shape parameter are defined as $\frac{h}{b} = 2$ and $\frac{b}{r} = 1$, respectively. This means that the tree crowns are modelled as spheres that are separated from the ground by half their diameter (Lucht et al., 2000a). The statistical fitting of the model to observations requires several measurements. Therefore, both Aqua and Terra MODIS instruments deliver input to the inversion process (Strahler et al., 1999; Lucht et al., 2000a). A back-up algorithm offers model inversions when only few observations are available. This algorithm makes use of the BRDF properties of previous full inversions and scales these shapes to new measurements. This back-up is termed magnitude inversion.

The respective MCD43A1 data sets contain the 3 resulting RTLSR model parameters at 500 m spatial resolution. Surface reflectances at arbitrary θ_v and θ_s can be modelled with these parameters. MCD43A2 data sets contain quality and auxiliary information. In this report the 4 quality levels are addressed as defined in Table 2.1. It should be noted that the quality is in decreasing order, i. e. level 1 represents the best quality. MCD43A4 data sets contain BRFs calculated from MCD43A1 RTLSR model parameters with $\theta_v = 0°$ and θ_s fixed to local solar noon. This means it has fixed viewing, but variable solar geometry. MCD43A4 are termed Nadir BRDF-Adjusted Reflectance (NBAR) products. All of the products contain data for the first 7 MODIS bands separately, which include visible, NIR and Shortwave Infrared (SWIR). They are available for all land areas from February 18, 2000 to just recently. The recent MODIS collection 5 offers MCD43A1 data sets with 8 day temporal resolution with phased production. This means it is produced every 8 days with data that was collected in 16 days.

For this study I downloaded MCD43A1, MCD43A2 and MCD43A4 data from the MODIS data pool (https://lpdaac.usgs.gov/) of between February 18, 2000 and November 25, 2013 and spatial tiles with horizontal numbers 10 to 13 and vertical numbers 8 to 9, i. e. 12 tiles in total, which cover northern South America.

2.4 Ground-based

Apart from spatial data, I made use of ground data as references for canopy processes. Ground data is usually used for validation purposes. Despite spatial mismatches between the represented areas between remote sensing and ground data (Turner et al., 2006), ground data is treated here as ground truth. Table 2.2 gives an overview of all ground sites, including the hereafter used abbreviations for the site names, the time span of data availability, and references for descriptions of equipment and surroundings. The positions of the ground sites can be found together with the landcover mask in Figure 3.1 on page 10.

I obtained data from two different kind of ground sites: Fluxtower and forest plots. The Fluxtower data was part of the LaThuile Fluxnet synthesis data set. Fluxnet is a worldwide network of micro-meteorological flux measurement sites and was specifically designed to validate MODIS Terra based estimates of net primary production (Baldocchi et al., 2001). At these sites Gross Primary Productivity (GPP) is measured with the eddy covariance technique. This is among the best practice approaches to assess GPP over long time periods on the ecosystem scale (Baldocchi, 2003). Alongside, air temperature at 2 m above ground and Photosynthetic Photon Flux Density (PPFD) is measured. I retrieved data with daily temporal resolution from the official Fluxnet site (http://fluxnet.ornl.gov/). Hereafter, Fluxtower locations are addressed with their official Fluxnet abbreviation, which always starts with BR for Brazilian locations (Table 2.2).

On the other hand, I obtained phenology data from long-term forest plots, which are part of the Global Ecosystem Monitoring network (GEM) (Doughty et al., 2014; Araujo-Murakami et al., 2014; Malhi et al., 2014). At all of them digital cameras with wide viewing angles capture incoming light. These measurements are used in a simple radiative transfer model to derive LAI (Doughty and Goulden, 2008). Additionally, in each plot litter fall was collected in 0.25 m^2 litter traps in 25 subplots. Leaf flush was calculated from the change in LAI and litter fall (Doughty and Goulden, 2008). All data from the forest plots was available on a monthly basis.

Table 2.2: Fluxtower and forest plots used in this study, fluxtower sites abbreviations start with BR

Full Name	Abbreviation	Data availability	Site description
Ecotone Bananal Island	BR-Ban	2003–2006	–
Caxiuanã Forest – Almeirim	BR-Cax	1999–2003	Carswell et al. (2002)
Rondonia – Rebio Jaru Ji Parana – Tower A	BR-Ji2	2000–2002	von Randow et al. (2002)
Manaus – ZF2 K34	BR-Ma2	1999–2006	Araújo et al. (2002)
Santarem – Km67 – Primary Forest	BR-Sa1	2002–2004	Saleska et al. (2003)
Caxiuanã – A, B	CaxA & B	2009–2010	Doughty et al. (2014)
Hacienda Kenia A & B	KenA & B	2009–2010	Araujo-Murakami et al. (2014)
Tambopata 5 & 6	Tam5 & 6	2009–2011	Malhi et al. (2014)

3 Methods

This chapter describes the methods used in this study. In Section 3.1 the definition and derivation of the study area mask is explained. As all analysis steps focus on different scales, the produced mask does not represent the study area, but rather the basis from which sub-masks with smaller extents were derived. Section 3.2 contains a description of how data availability was investigated in this study. This step was necessary to adapt later analysis as well as judge the reliability of results. Finally, the three core analyses are explained in Section 3.3 to 3.5. They follow the logical order of the research questions in Chapter 1. Next to EVI, I prepared some of the core analyses also with the NDVI. It was interesting to compare this more intensely studied index compares to EVI.

Generally, all methods described here were built around the MODIS MCD43 product suite. This implies that all temporal operations were adjusted to the temporal resolution of MCD43 products, which is quasi 8 daily. The time steps corresponding to this resolution are referred to as (MODIS) intervals in the following. The temporal range was restricted by the combined availability of the vegetation index and precipitation data sets. This range was from February 18, 2000 until November 9, 2013.

3.1 Definition of landcover mask

The aim of this study was to investigate undisturbed tropical forests in the Amazon basin. For this reason I generated a spatial mask, which is the product of two data sets. First, the IGBP land cover classification contained in the MCD12Q1 product defined evergreen broadleaf forests. Second, the LBA hydrological river basin map depicted the study area's outer boundary. I integrated the full time series of available MCD12Q1 classifications to ensure choosing only pixels with a stable landcover over time. To be considered part of the study area a pixel has to fulfil these criteria:

1. The pixel has to be within the Amazon river basin,
2. all available classifications need to be evergreen broadleaf forest, and
3. at least two thirds of the 12 observations need to be of good quality according to the MCD12Q1 quality flags.

The MCD12Q1 product is not available in 2000 and 2013. However, I expected most areas that were evergreen broadleaf forest between 2001 and 2012 also to be it in 2000 and 2013. The error introduced with this assumption should be low. The product of this masking process was used as a basic mask for further analysis. The following separate analysis steps focus on subregions within this major study area.

Figure 3.1 shows the final landcover mask, considered as Amazon rainforest in this study. The hydrological basin had an approximate size of $6 \cdot 10^6\,\mathrm{km}^2$. The area included into the mask had a size of $\sim 4.5 \cdot 10^6\,\mathrm{km}^2$. Soares-Filho et al. (2006) estimated this area to be $5.3 \cdot 10^6\,\mathrm{km}^2$.

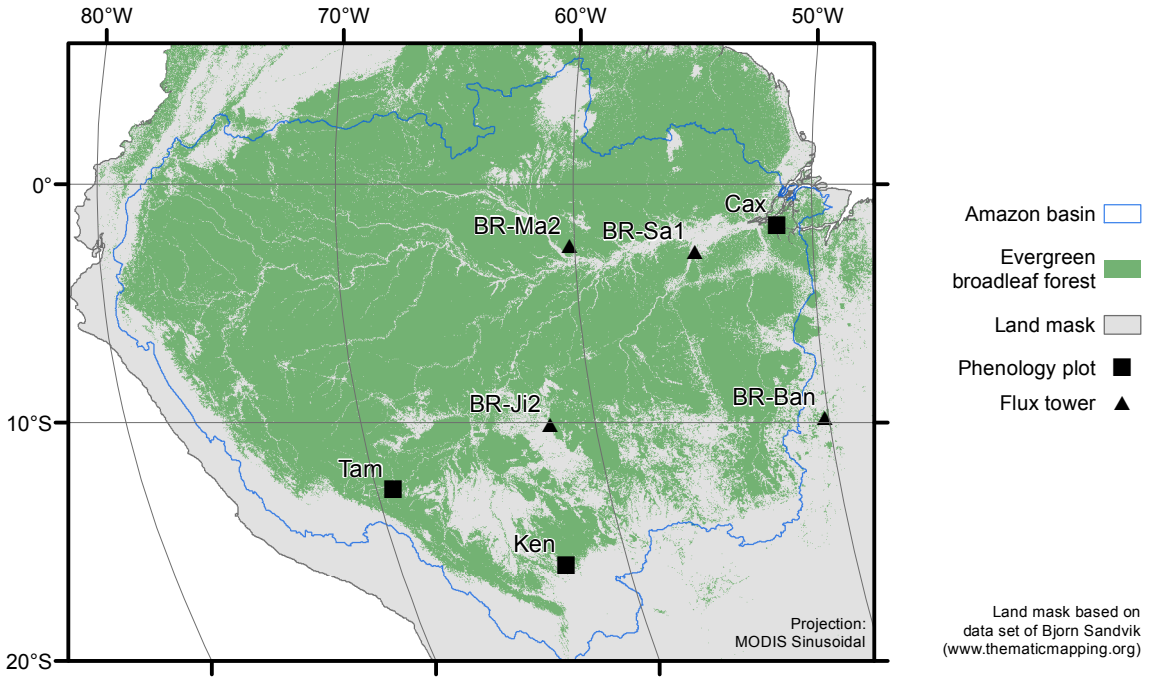

Figure 3.1: Study area spatial mask and individual ground validation sites used in this study, mask defined as regions of evergreen broadleaf vegetation within the Amazon basin between 2001 and 2012, explanations for abbreviations for ground sites can be found in Table 2.2

The difference may be explained by the restrictive masking procedure used here. This likely produced a high number of false negative classifications, i. e. pixels which were not considered rainforest, but in fact should be. However, this conservative approach ensured higher accuracy for positive forest classifications. Apart from the mask, Figure 3.1 shows the locations of fluxtowers and phenology plot sites throughout the Amazon basin that were addressed in this study (Section 2.4). The fluxtower site Ecotone Bananal Island (BR-Ban) made up an exception, since it lies outside the Amazon basin. Nonetheless, it is surrounded by dense tropical forest.

3.2 Data density

Up to now, the MCD43 product suite has not been regularly used in Amazon vegetation studies. In contrast to the MOD13 and MYD13 vegetation indices, MCD43 requires a higher number of observations. This made it necessary to conduct an assessment of the available data density over the Amazon basin to judge the reliability of further analysis, especially in the temporal dimension. The vegetation index analysis focused on EVI, so I evaluated the band 1 (red), 2 (NIR) and 3 (blue) MCD43A2 quality flags. I defined the quality of resulting EVI values as the lowest quality of the blue, red and NIR band.

To assess spatial quality patterns, I produced quality maps for the Amazon basin. Each pixel of these maps represents the fraction of observations in the hyper-temporal image cube, which fulfils the quality criterion, in relation to the total number of observations. I focused on quality level 2, which involves only full inversions, and level 4, which can include inversions made with 3 observations, the minimal required number of observations. Apart from these maps, I chose

distinct, small subregions to gain insight into temporal patterns of data density. For that I counted the number of pixels, which fulfilled the given quality criterion, for each subregion and interval. This signal over time gives insight into when data availability is high and low.

3.3 Seasonal changes in canopy greenness and structure

I prepared several time series to analyse seasonal changes in canopy greenness and structure. This aimed at studying impacts of SSGEs on spectral indices and to provide an approach independent from that of Morton et al. (2014). To make my results comparable to Morton et al. (2014), I selected MODIS tiles h11v09 and h12v09 as the study area. I screened all data sets with the MCD43A2 quality flags to mask out qualities below level 2 (explanation see Table 2.1). Then I applied the landcover mask described in Section 3.1 to focus on evergreen broadleaf forests. Furthermore, I averaged the respective mosaics spatially to obtain one temporal value per MODIS interval. All temporal values make up the time series. In contrast to Morton et al. (2014), who obtained BRDF modelling results on a monthly basis, my time series have 8 day temporal resolution.

The first time series sets were NBAR NIR reflectance, NDVI and EVI. I explicitely produced NIR time series to investigate their relationship to EVI. Galvão et al. (2011) emphasize the high dependence of EVI on NIR reflectance. To retrieve these products, I extracted blue, red and NIR bands from the MCD43A4 NBAR product. While the View Zenith Angle (VZA) is kept constantly at nadir for this product, the SZA follows the SZA at local solar noon and thus varies over the course of the year. Then, I derived NDVI and EVI, which are defined as:

$$NDVI = \frac{\rho_{NIR} - \rho_{red}}{\rho_{NIR} + \rho_{red}} \tag{3.1}$$

$$EVI = 2.5 \times \frac{\rho_{NIR} - \rho_{red}}{\rho_{NIR} + 6\,\rho_{red} - 7.5\,\rho_{blue} + 1} \tag{3.2}$$

The second set of time series consisted of BRDF-adjusted NIR reflectance, NDVI and EVI. The MCD43A1 product represents an approach for BRDF modelling and thus fully accounting for sun-sensor-geometry effects independent from Morton et al. (2014). I derived BRFs for the blue, red, and NIR band with the RTLSR model parameters contained in MCD43A1 and the RTLSR model equations (Section 2.3). The reflectances were modeled at $\theta_s = 30°$ and $\theta_v = 0°$.

Third, I extracted the SZA at local solar noon, which is contained in the MCD43A2 product as an auxiliary variable. Galvão et al. (2011) underline the high correlation between NIR/EVI and SZA, which leads to apparent green up in time series. Taken this, SZA should highly correlate with NIR and EVI.

Besides reflectance based metrics I investigated the RTLSR model parameters themselves. They theoretically contain structural information about the canopy (Chopping, 2008), although only few studies have directly tested these relationships yet. The volumetric parameter f_{vol} is exponentially related to LAI (Lucht et al., 2000b) and the geometric parameter f_{geo} to within canopy shadowing effects, thus to the crown density or canopy gap fraction (Strahler et al., 1999). To have a look into the temporal patterns of the RTLSR parameters, I produced time series of the them for MODIS bands 1 (red) and 2 (NIR). I applied the same spatial processing as for the reflectance bands and indices described above.

3.4 Relationship of canopy greenness to carbon uptake and phenology

Previous studies successfully used EVI in forest carbon uptake models (Xiao et al., 2004b, 2005). Thus, EVI is generally treated as a proxy for GPP (Brando et al., 2010), but also for canopy structure and LAI (Gao et al., 2000). However, these studies base their analysis on EVI data that is not corrected for SSGEs. The risk here is that uncorrected EVI only correlates well with ground processes, because of its annual periodicity induced by the changing SZA. So the question appears if EVI–ground relationships can be found with BRDF-adjusted EVI as well? The aim here was to provide a small scale validation based on ground data, and comparison of the predictive performance of NBAR and BRDF-adjusted EVI. Surely it is not meant as a conclusive analysis, but as a first indication how BRDF correction influences the predictive power of EVI concerning canopy processes for Amazon forests. For this purpose, I conducted two independent analyses: one relating EVI to GPP as an indicator for canopy carbon cycling, the other relating EVI to canopy structural characteristics.

The satellite data preprocessing was the same for both analyses. For all sites, I extracted spatial windows from the hyper-temporal EVI cubes resulting in smaller spatial cubes. The seasonal dynamics within the windows were assumed homogenous. Since low data density for high quality BRDF inversions was a major issue at all ground validation sites (Section 4.1), I chose the quality requirement to be only level 4. I chose a window size of 3 × 3 km or 6 × 6 pixels. Pixels within this window were also masked with the landcover mask. For each MODIS interval I calculated mean EVI.

3.4.1 Carbon uptake coupling

EVI is only a proxy for GPP. In fact, EVI is sensitive to absorption of Photosynthetically Active Radiation (PAR) by chlorophyll (Huete et al., 2011), but this does not reflect the actual rate of vegetation carbon uptake. Local meteorological conditions, such as temperature and water availability, restrict the photosynthesis rate. This makes it necessary to translate EVI into GPP by considering the given meteorological constrains.

For this reason I employed a carbon uptake model that digests remote sensing and meteorological measures to estimate GPP. Its name is Vegetation Photosynthesis Model (VPM) (Xiao et al., 2004b,a, 2005). The rationale behind this approach was to run the model with both NBAR and BRDF-adjusted spectral indices, and compare their performances with GPP measured with eddy covariance method. When the model equations are well defined and only the spectral data input differs, the BRDF-adjusted indices should perform better, since they exclude artifacts of SSGEs. Here I talk about indices in plural, because the VPM involves not only EVI, but also the Land Surface Water Index (LSWI). Nonetheless, also the LSWI was calculated in its NBAR and BRDF-adjusted from parallel to EVI to keep the two model versions consistent.

In the following the VPM equations are repeated to show the role of EVI, LSWI and other meteorological parameters. VPM models GPP as (Xiao et al., 2005):

$$GPP = \varepsilon_g \times FAPAR_{PAV} \times PAR \tag{3.3}$$

$$\varepsilon_g = \varepsilon_0 \times T_{scalar} \times W_{scalar} \times P_{scalar} \tag{3.4}$$

where PAR is the photosynthetically active radiation ($\mu mol\, m^{-2}\, d^{-1}$, PPFD), $FAPAR_{PAV}$ the unitless fraction of PAR absorbed by Photosynthetically Active Vegetation (PAV), ε_g the Light Use Efficiency (LUE) ($g\, C\, \mu mol\, PAR^{-1}$), and ε_0 the maximum LUE ($g\, C\, \mu mol\, PAR^{-1}$). In VPM $FAPAR_{PAV}$ is estimated as a linear function of EVI with the coefficient a set to 1.0:

$$FAPAR_{PAV} = a \times EVI \tag{3.5}$$

T_{scalar}, W_{scalar} and P_{scalar} are scalars that constrain maximum possible LUE by temperature, water and phenology effects, respectively. T_{scalar} follows the definition of the Terrestrial Ecosystem Model (Raich et al., 1991):

$$T_{scalar} = \max\left(\frac{(T - T_{min})\,(T - T_{max})}{(T - T_{min})\,(T - T_{max}) - (T - T_{opt})^2},\, 0\right) \tag{3.6}$$

W_{scalar} is a function of the LSWI. LSWI is an index sensitive to vegetation water content and uses the water sensitive MODIS SWIR band at 1628–1652 nm (Xiao et al., 2004b,a):

$$LSWI = \frac{\rho_{NIR} - \rho_{swir}}{\rho_{NIR} + \rho_{swir}} \tag{3.7}$$

$$W_{scalar} = \frac{1 + LSWI}{1 + LSWI_{max}} \tag{3.8}$$

where $LSWI_{max}$ is the maximum LSWI within the plant growing season.

P_{scalar} adjusts for canopy phenology. Phenology influences maximum LUE depending on the phenologcial status of plants. Since tropical forests in the Amazon basin carry green foliage all year, P_{scalar} is simply assumed as 1.

The model parametrization here was adopted from Xiao et al. (2005). This means ε_0 is 0.54 $g\, C\ \mu mol\, PAR^{-1}$, T_{min} is 2°C, T_{opt} is 28°C, T_{max} is 48°C, and $LSWI_{max}$ is the maximum LSWI observed in the whole LSWI time series. The actual temperature T and PPFD were measured at the fluxtowers. Remote sensing products integrated in the model were EVI and LSWI. As stated before, I compared two versions of preprocessing, NBAR and BRDF-adjusted for $\theta_s = 30°$ and $\theta_v = 0°$. LSWI-preprocessing was the same as for EVI. For validation purposes I used GPP measured at the fluxtowers with the eddy covariance technique. I aggregated all ground based time series to match the 8 day MODIS intervals. Only when there was data available for all VPM inputs as well as GPP derived from eddy covariance measurements the respective interval was taken into account. All ground based data sets were equal for both model versions of remote sensing preprocessing, so that differences between NBAR and BRDF-adjusted remote sensing indices were emphasised.

3.4.2 Phenological coupling

The comparison of EVI with canopy structural parameters is less straightforward. For instance, EVI is treated as non-linearly related to LAI, so that similar LAI conditions can produce different values of EVI (Huete et al., 2002). However, EVI is treated as highly sensitive to dry season leaf flush, because of increasing canopy NIR reflectance and LAI (Samanta et al., 2012c). Dry season leaf flush was observed in several ground based studies (Doughty and Goulden, 2008; Brando et al., 2010; Malhi et al., 2014). So with EVI under question due to possible SSGEs, the leaf flush–EVI coupling was tested here.

I compiled linear regression models with leaf flush derived from forest plots as an independent and EVI as the dependent variable. The rationale behind was that leaf flush should have an instantaneous impact on the EVI signal mostly by increased NIR reflectance. Additionally, I incorporated the SZA at local solar noon as an independent variable to check its predictive power on a local scale. This is supplementary to Section 3.3, where I investigated this on a coarse scale. As in Section 3.3, I extracted SZA at local solar noon from the MCD43A2 product parallel to the data necessary for EVI. The models were set up for each forest plot individually and formulated as:

$$EVI_i = \beta_0 + \beta_1 Leaf flush_i + \beta_2 SZA_i + \varepsilon_i \tag{3.9}$$

where EVI_i is the NBAR and BRDF-adjusted EVI, respectively, $Leaf flush_i$ is leaf flush, SZA_i the solar zenith angle, and i the index of the interval. Since all phenological measures had monthly resolution, I aggregated the remote sensing data by temporal averaging to match this. A disadvantage of the linear regression approach is that the error term ε_i will contain temporal auto-correlation, which is typical for time series data. This raises significance of regressors, so that significant relationships have to be interpreted carefully.

3.5 Impact of water stress on dry season greenness

In coarse scale assessments of drought impacts on Amazon rainforests it proved helpful to analyse standardized anomalies of remote sensing products during drought periods (e.g. Anderson et al., 2010; Xu et al., 2011; Saatchi et al., 2013), i. e. the standardized deviation of a remote sensing metric from its long-term average. This is defined as (Xu et al., 2011):

$$a_i = \frac{x_i - \bar{x}}{\sigma(\langle x \rangle)} \tag{3.10}$$

where $\langle x \rangle$ is the vector of observations, x_i is the value of a time series at time step i, $\bar{x}$ is the long-term mean and $\sigma(\langle x \rangle)$ is the standard deviation of $\langle x \rangle$. If the anomalies are only calculated for certain periods of the year, they are called seasonal anomalies. The idea behind this approach is that the remote sensing metric, which is treated as a proxy for canopy functional status, shows abnormal deviations from the mean during abnormal years, for example drought years. The advantage of using standardized anomalies is that they make different sites with different base levels and variability of the remote sensing measure comparable. Additional to the spectral information, this approach can be applied on a measure for dry season intensity. Since the resulting data set of anomalies is unitless as are the spectral anomalies, both data sets can be easily compared to each other.

I made use of the standardized anomaly approach to investigate the general greenness response expressed as EVI to drought conditions. The novelty of my approach is the investigation of the greenness response over multiple years using spectral data corrected for SSGEs. Moreover, I utilize not only a relative but also an absolute drought index. Next, I describe first the preprocessing for the EVI and precipitation data, second the idea behind the drought indices and how they are computed, and finally how EVI and drought metrics were implemented in this study and how they were compared.

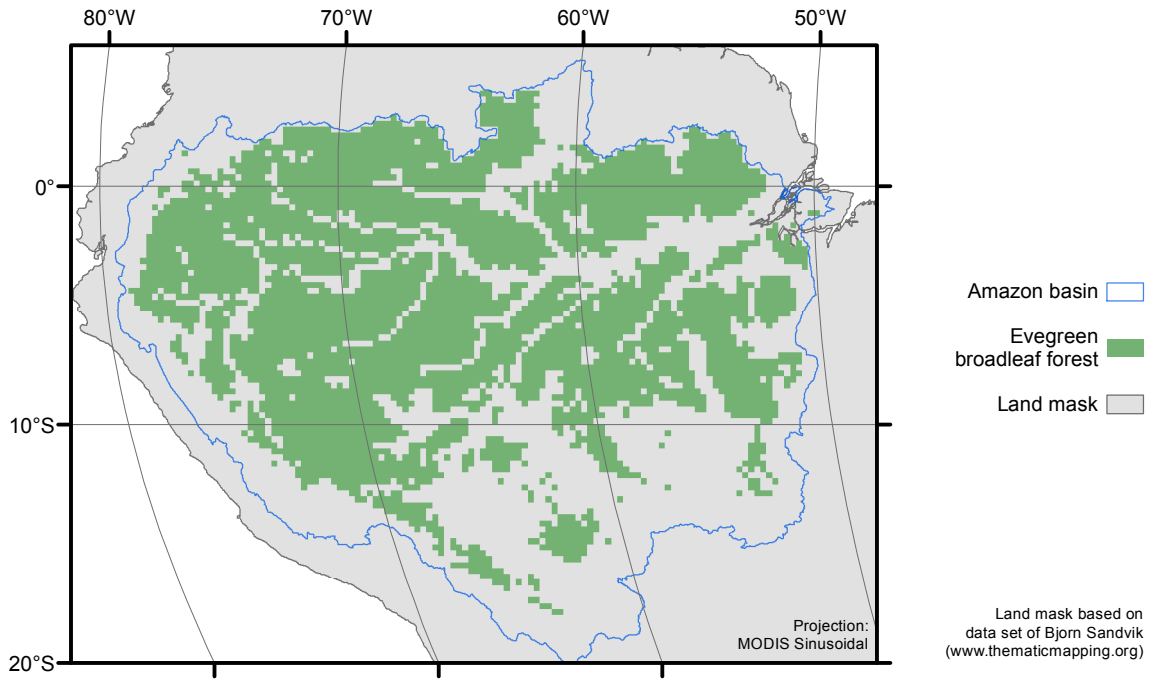

Figure 3.2: Aggregated Landcover mask, 30 km (~0.25°) resolution

3.5.1 Preprocessing

I spatially aggregated MODIS-based data to 30 km (~0.25°) resolution to match the resolution of TMPA-based precipitation and to increase data availability within each pixel. First, I needed to aggregate the landcover mask. The requirement for valid aggregated forest pixels was that more than 90% of pixels in the underlying 500 m landcover mask must be valid forest pixels as defined in Section 3.1. The aggregated mask can be seen in Figure 3.2. This mask defined valid pixels for the analysis of drought impacts. For each forested 30 km pixel, covered 500 m-BRDF-adjusted EVI pixels were quality filtered (level 2), landcover masked, and averaged. With the BRDF-adjustment and quality level 2 the focus on this part of the analysis was to use best estimates of canopy greenness and assess its response to drought.

The aggregation process can be regarded critical as it removes spatial variability within large areas. Additionally, it means summarizing vegetation greenness dynamics on artificially selected grids. However, 30 km pixel size is close to TMPA's native resolution; so processing on a finer scale would have meant to resample the data, which results in extrapolating trends to finer scales. Nonetheless, this is a moderate aggregation compared to those applied for example by Samanta et al. (2012c), Saatchi et al. (2013) or Morton et al. (2014).

The TMPA needed to be aggregated temporally to match MODIS intervals, so that each grid cell represents 8 day intervals. All further steps use this 8 day resolution. In fact, MODIS data represents 16 day intervals with phased production (Section 2.3), so aggregated precipitation intervals do not exactly correspond to these intervals. Nevertheless, non-overlapping data is conceptually clearer in further processing, which is why I decided for this way.

The result of these preprocessing steps were two hyper-temporal data cubes with 30 km spatial and 8 day temporal resolution spanning the same spatial extent and time.

3.5.2 Drought indices

A drought index is a "computed value which is related to some of the cumulative effects of a prolonged and abnormal moisture deficiency [...]" (WMO/UNESCO, 2011). In the context of droughts in the Amazon forests the principal requirement for a drought index is its ability to represent how water shortage influences the vegetation. In this study two different types of drought indices have been used: the Standardized Precipitation Index (SPI), which expresses relative drought, and the Maximum Cumulative Water Deficit (MCWD), an absolute drought index. Furthermore, I assumed dry season to be between July and September, a simplification applied by several other studies as well (Samanta et al., 2012c).

The SPI was introduced by McKee et al. (1993). Its computation is similar to that of seasonal standardized anomalies: A moving window of a given width, say 6 months, runs over the precipitation time series. For each monthly step that it makes it fits the precipitation observations of this month plus the past 5 months of this year and the historical data to a gamma distribution. Then the deviation of the precipitation for the month in focus can be determined. The SPI can be interpreted in terms of occurrence probability of a given precipitation amount compared to historical data, which makes it a relative drought index. Positive and negative values mark anomalously wet and dry months, respectively. For instance, an SPI $\leq$ -2 marks an extreme drought (McKee et al., 1993).

On the other hand, the MCWD, proposed by Aragão et al. (2007), is an absolute drought index. This is because it uses a physiological meaningful evapotranspirational demand of tropical forests, which is assumed to be the same for all tropical forests. It is estimated as 100 mm month^{-1}. Additionally, the MCWD accounts for the accumulative effect of ongoing dry spells. To obtain MCWD first the Water Deficit (WD) per time interval has to be calculated. The original formulation of Aragão et al. (2007) for WD is:

```
If WD_n-1(i,j) - E(i,j) + P_n(i,j) < 0
then WD_n(i,j) = WD_n-1(i,j) - E(i,j) + P_n(i,j)
else WD_n(i,j) = 0
```

which is simply:

```
WD_n(i,j) = min(WD_n-1(i,j) - E(i,j) + P_n(i,j), 0)
```

where WD_n is the water deficit at interval n, E the evapotranspirational demand, P_n the precipitation at interval n, and (i,j) the pixel indices. During preliminary tests I discovered that WD accumulates during dry seasons in southern regions of the Amazon forests and cannot be counterbalanced by precipitation in the wet season. Physically this would mean an overall drying trend. In this case the evapotranspirational demand of 100 mm month^{-1} is probably overestimated. In accordance with the verbal formulation in Saatchi et al. (2013) I reformulated the algorithm, so that WD_n is reset to 0 if precipitation exceeds the evapotranspirational demand:

```
If P_n(i,j) - E(i,j) < 0
then WD_n(i,j) = WD_n-1(i,j) - E(i,j) + P_n(i,j)
else WD_n(i,j) = 0
```

MCWD is defined as the absolute value of the minimum WD in a year, so that $MCWD \geq 0$ and higher values mean stronger drought.

3.5.3 Integration

Using the hyper-temporal EVI and TMPA data cubes, I applied the following steps to each 30 km-pixel independently. I seasonally averaged EVI for September for each year separately, then transformed this vector into standardized anomalies (Eq. 3.10). This produced 14 values per pixel belonging to the 14 years of input data. I focused on September, because this is the last dry season month, so impacts should be highest during this month. Moreover, I calculated SPI for September for each year based on a 6 months moving window. This time period emphasises the difference between dry and wet season, and was already used by another study investigating droughts in the Amazon basin (Li et al., 2008). For the calculation of MCWD for 8 day intervals, I translated the evapotranspirational demand into 26.28 mm interval^{-1}. Other than for SPI, I applied the MCWD algorithm on precipitation data starting in January and ending in September in each year. This means that the value represents the MCWD for the months January to September. In this way potentially higher values of MCWD that appear after September were omitted; eventually they do not influence EVI in September.

To compare the reaction of EVI anomalies to droughts, I set up linear regression models for each drought index. The September EVI standardized anomaly $EVI_{anomaly}$ was the dependent variable, and September SPI and yearly MCWD were the regressors, respectively:

$$EVI_{anomaly,i} = \beta_0 + \beta_1 DI_i + \varepsilon_i \tag{3.11}$$

where DI_i denotes the respective drought index and ε_i the error term. I evaluated the regressions for the two drought indices in two different ways, so that i has two different meanings. On the one hand, I applied the regressions on the 30 km-pixels, so that i represents the year. 14 pairs of $EVI_{anomaly}$ and drought index were available for each pixel. I prepared maps that contain the values of the slope parameter β_1 and the p-value for this slope. In this way it was possible to assess the EVI response to the drought index on a very fine scale.

Additionally, I conducted the linear regression on a tile basis. This means I used all available $EVI_{anomaly}$–drought index pairs over all years of a whole MODIS tile to build the regression model. In this way it was possible to evaluate the relationship's form – for instance if it is actually linear – while still retaining a coarse spatial resolution. To visualize this I created scatterplots that resemble the MODIS tiles over the Amazon basin. Of course, the spatial subsetting according to the tiles is arbitrary in respect to ecological regions. However, it still represents spatial differences in the $EVI_{anomaly}$–drought index coupling. Moreover, it produces more meaningful statistical models than the pixel-based approach since it uses many more points.

4 Results

This chapter presents and describes the results obtained from the methods presented in Chapter 3. Section 4.1 shortly investigates the density of available data. Sections 3.3 to 3.5 follow the order of the research questions given in Chapter 1.

4.1 Data density

Figure 4.1 displays available MCD43A data density with a spatial resolution of 500 m for quality levels 2 and 4 as defined in Table 2.1. The maps are not masked with the major study area mask to show the overall spatial trend. The availability is relative to the total number of 632 available MODIS intervals. Both quality levels exhibit a spatial trend in N-S direction: density is lowest around the equator and increases north- and southwards. Moreover, fewer observations were available at the Andean foothills and slightly fewer in the western compared to eastern regions of the basin. Despite these spatial gradients, the strongest difference was between quality levels 2 and 4. While average availability for all visible tiles and landcover types was 57.8% for level 4, it was only 25.8% for level 2. This strongly hampers time series analysis with the MCD43A product for the Amazon basin, if high quality is required.

Figure 4.2 shows data density time series for the Manaus fluxtower (BR-Ma2) and the Kenia forest plot (Ken A) sites. Both time lines summarize squares of 3 × 3 km (6 × 6 pixels) around the locations, i. e. 36 MODIS pixels. This means that if data availability was 100% for an interval, all 36 observations around the point location had the respective quality. Both

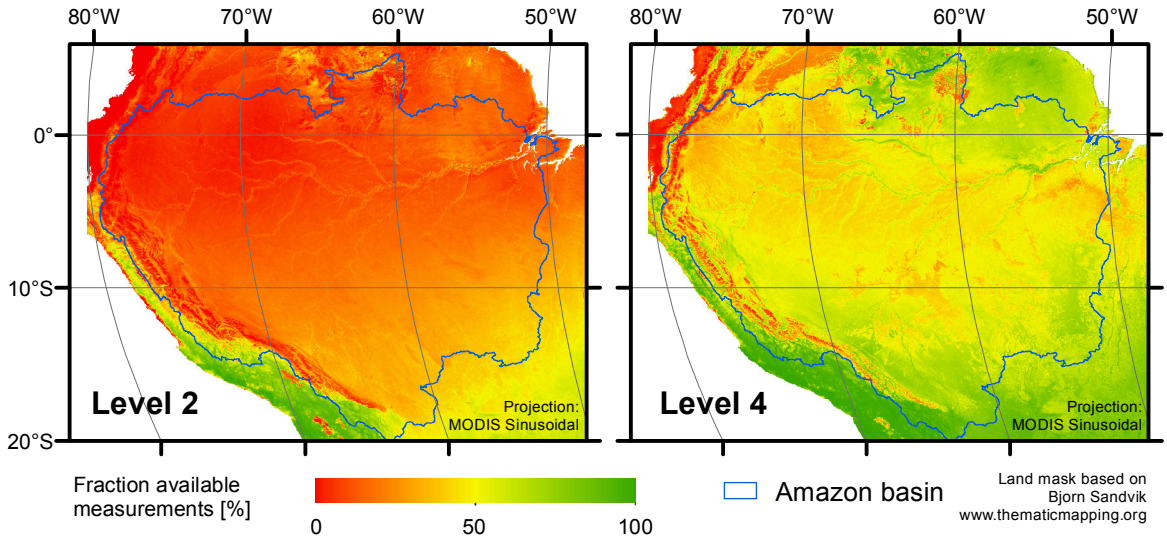

Figure 4.1: Density of valid MCD43 observations between Feb 18, 2000 and Nov 25, 2013 over the Amazon basin for quality level 2 and 4 (definitions see Table 2.1)

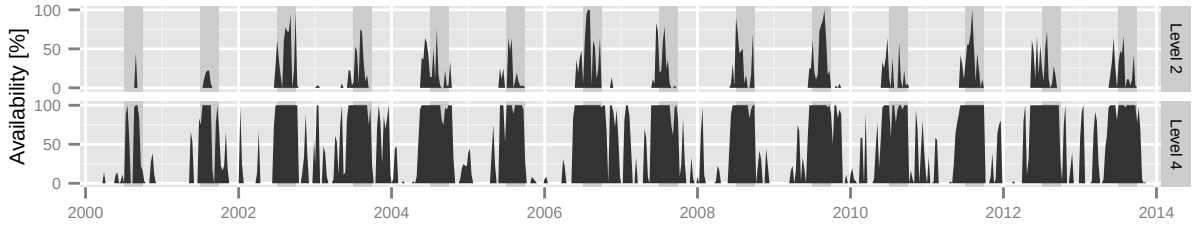

(a) BR-Ma2

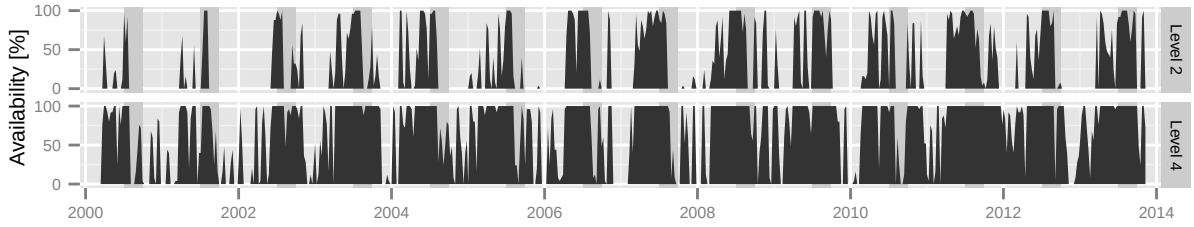

(b) Ken A

Figure 4.2: Valid MCD43 observations densities between Feb 18, 2000 and Nov 25, 2013 for a neighborhood of 3 × 3 km (~6 × 6 pixels) around two locations in the study area, grey bands indicate typical dry seasons (July to September)

time series showed seasonal patterns with high densities during austral winter (JJA) and low densities down to no observations during austral summer (DJF). Additionally, both showed a much higher availability for quality level 4 than for 2, which is comparable to Figure 4.1. The availability was generally lower before 2002. This was the year when MODIS on the Aqua platform was brought into orbit and approximately doubled the chances for good quality observations. The main difference between both locations was an overall higher data availability for the Kenia site, which can be expected when considering Figure 4.1. At the Manaus site data availabilities over all intervals were 9.3% and 56.0% for level 2 and 4, respectively. For the Kenia site they were 21.9% and 77.1%, respectively.

4.2 Seasonal changes in canopy greenness and structure

Figure 4.3 shows spatially averaged BRFs and vegetation indices time series with 8 day temporal resolution, which emulate the results of Morton et al. (2014). From the start of the time line until circa 2002 occasional gaps appeared, when no data was available for the whole study area. Additional observations by MODIS on Aqua after 2002 explain the fewer gaps, which is comparable to results in Figure 4.2. The data density time line for the h11v09 and h12v09 tiles (not shown) resembled Figure 4.2 with only very few observations during the wet season. The total number of pixels involved in analysis was 914 730 869, which is around 4 500 times larger than the number Morton et al. (2014) used. A longer study period, higher temporal sampling and higher spatial resolution used in this study accounted for this difference.

NBAR and BRDF-adjusted NDVI time series agreed well with each other. NBAR NDVI was generally lower than BRDF-adjusted NDVI. However, both NDVI curves followed each other closely. This points to a higher stability of NDVI against directional effects. Occasionally, NDVI strongly dropped during the dry season, especially in 2007 and 2010. Furthermore, EVI

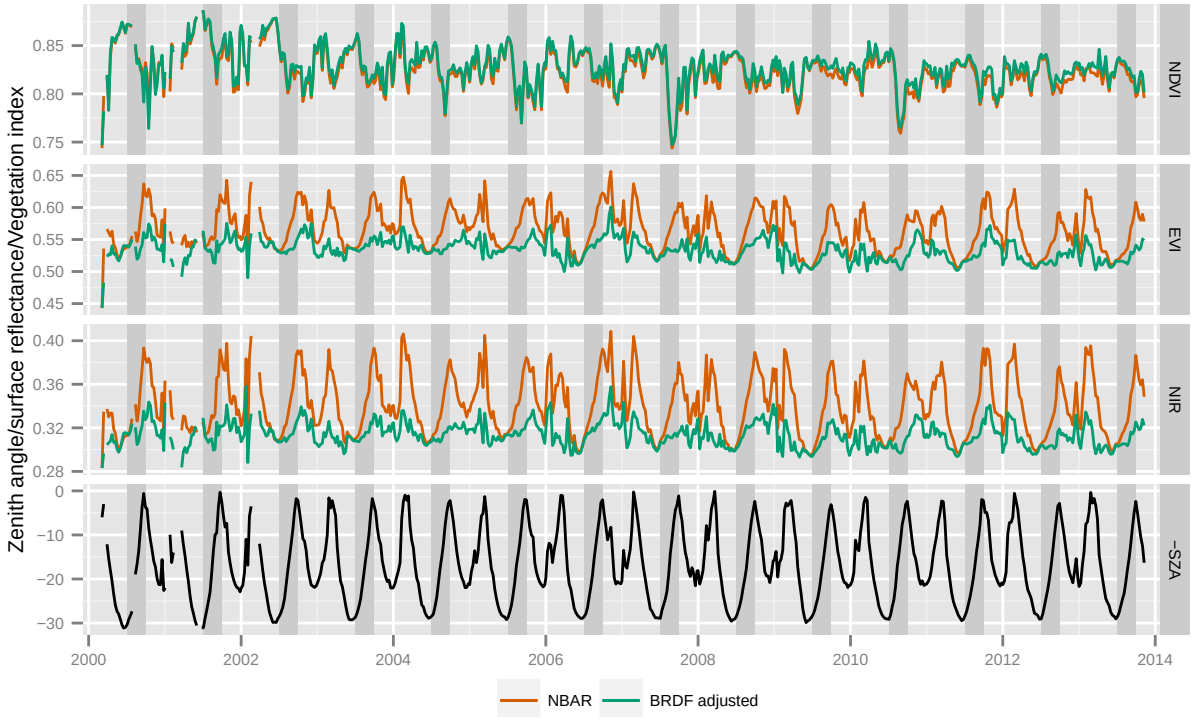

Figure 4.3: Spatially averaged viewing zenith angle (NBAR) and viewing and sun zenith angle adjusted (BRDF-adjusted) NDVI, EVI and NIR for MODIS tiles h11v09 and h12v09, lines connect data points, solar zenith angles are reversed to facilitate comparison with vegetation index trends, 8 day temporal resolution, grey bands indicate typical dry seasons (July to September)

and NIR reflectance followed the same trends for both irrespective of the processing type. The Kendall correlation coefficients between EVI and NIR reflectance supported this, with values of 0.875 and 0.819 for NBAR and BRDF-adjusted processing, respectively. Kendall's rank correlation coefficient, or Kendall's τ, is a statistical measure for correlation used in time series analysis, which ranges ranges from -1 (negative association) to 1 (positive association) (de Jong et al., 2011). High values showed the strong dependence of EVI on NIR reflectance.

Another dependence was the one between SZA and NBAR NIR reflectance. As seen in Figure 4.3 NBAR NIR reflectance followed the SZA without a temporal lag. Even the two peaks around the turn of the year occurred in both time series. The SZA pattern marks the sun's apparent movement during the course of the year: The equinoxes occur on September 23 and March 20, and result in the lowest SZAs. A low Kendall's τ between SZA and NBAR NIR reflectance of -0.725 underlined this strong and reversed relationship. The SZA–NIR reflectance coupling was especially strong in the NBAR product, because it uses the SZA at local solar noon as an input for θ_s in the RTLSR model.

On the other hand, this coupling was much weaker for the BRDF-adjusted NIR reflectance and EVI. The double peak structure of SZA did not appear in all years for the BRDF-adjusted NIR reflectance. Additionally, the magnitude of change during austral summer was much lower compared to NBAR processed products. A relatively low Kendall's τ of -0.325 between BRDF-adjusted NIR reflectance and SZA underpinned this weaker coupling. An explanation

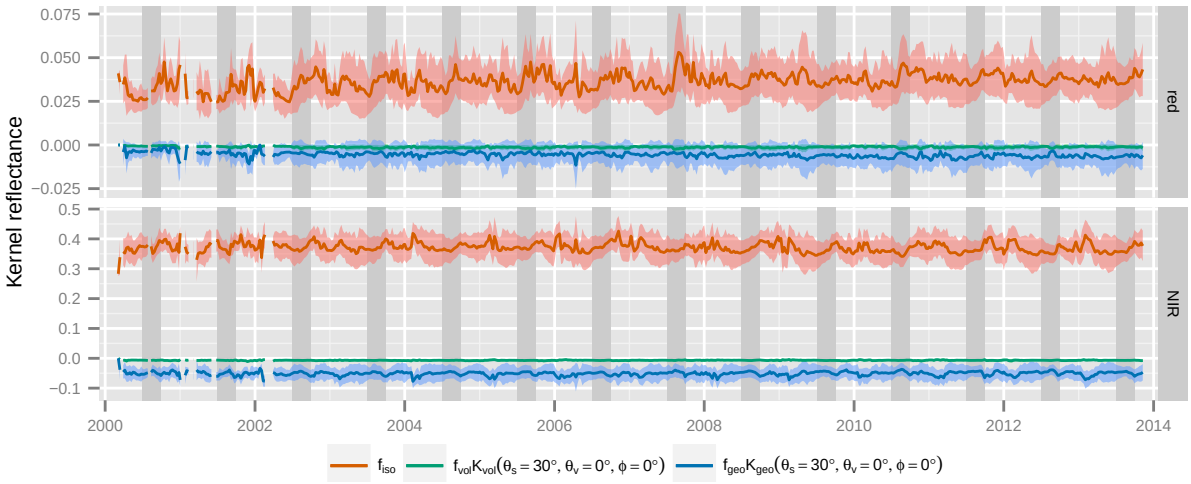

Figure 4.4: Spatially averaged RTLSR-model terms for MODIS tiles h11v09 and h12v09 for $\theta_s = 30°$, $\theta_v = 0°$ and $\phi = 0°$, coloured areas are ±1 sd around the mean, 8 day temporal resolution, grey bands indicate typical dry seasons (July to September)

for this is that the BRDF-adjusted NIR reflectance used a fixed θ_s, so that a direct impact of the SZA on NIR reflectance should not be possible. However, a weak relationship existed.

Concerning seasonality, I compared the seasonal average of months September to December with the other months with a one sided two sample Student's t-test. The values for September to December were significantly higher ($p < 0.01$). The arithmetic mean for all observations between September to December was 0.542, while it was 0.525 for all other months. Although the used t-test does not account for temporal auto-correlation and might thereby overestimate differences, this result still points to a seasonal difference in canopy greenness. Also NDVI, which appeared to be hardly influenced by SSGE, showed seasonality as seen in the curves, although with opposite trends compared to EVI.

The question arose if these temporal patterns were artifacts of spatial aggregation, since the h11v09 and h12v09 tiles cover a vast area of approximately $1.44 \cdot 10^6\,\mathrm{km}^2$. However, I also investigated time series on finer scales, namely around the BR-Ma2 (Figure A.1) and BR-Ji2 (Figure A.2) flux towers. These time series confirmed the robustness of NDVI against directional effects. Furthermore, I found generally lower values for BRDF-adjusted than for NBAR EVI and increasing EVI during the dry season comparable to the coarser scale analysis. I could not investigate the behaviour at the beginning of the year with certainty due to missing data. Nonetheless, the temporal patterns found in the coarse scale analysis did not appear to be artifacts of spatial aggregation.

Switching to the the analysis of the underlying RTLSR model parameters, Figure 4.4 shows spatially averaged values of the RTLSR terms extracted from the MCD43A1 product for the red and NIR bands over MODIS tiles h11v09 and h12v09. Model terms in this respect means that the model parameters f_{vol} and f_{geo} were multiplied with the respective values of the RossThick and LiSparse kernels for $\theta_s = 30°$, $\theta_v = 0°$ and $\phi = 0°$. In this way the single curves represent the contribution of isotropic, volumetric and geometric scattering to the overall signal in each band at this specific sun and viewing geometry: Their per band added values correspond to the reflectances that were used to derive NDVI and EVI in Figure 4.3.

Although seasonal variation in the time series was not as obvious as in the case of reflectances and indices, some seasonal patterns could be identified. First of all, isotropic scattering had generally the highest contribution to the reflectance signal for both bands and at all times. This is why its seasonality influences the reflectance most. Generally, values increased during the dry season resulting in peak values at the end of September, especially for the NIR band. Following the leaf flush argumentation this pattern could be triggered by replacement of upper canopy leaves with new leaves that are less populated by epiphylls and have higher NIR reflectance (Toomey et al., 2009). However, the curve also followed the SZA, so that a peak at the end of September and at the beginning of the year could be observed. Isotropic reflectance in the red band also followed the SZA pattern.

The other two terms played a much smaller role with the simulated observation geometry ($\theta_s = 30°$, $\theta_v = 0°$, $\phi = 0°$). Volumetric scattering had only a minor, negative contribution to reflectance for both bands. This is because the value for the RossThick kernel is negative while the parameter f_{vol} is always positive. Physically this can be interpreted as low influence of volume scattering at low SZA and VZA. Geometric scattering had a negative contribution in both bands. This stems from shadowing effects that reduce the reflectance. These already occur with small changes in viewing and/or solar geometry.

4.3 Relationship of canopy greenness to carbon uptake and phenology

Figure 4.5 shows GPP modelled with VPM (Xiao et al., 2005) compared to GPP measured with the eddy covariance method at five fluxtower locations. The VPM was driven by NBAR and BRDF-adjusted EVI and the same ground data for each location. I assessed the model performance with linear regression models for each site and EVI version individually:

$$GPP_{measured,i} = \beta_0 + \beta_1 GPP_{modelled,i} + \varepsilon_i \tag{4.1}$$

where $GPP_{measured,i}$ is the measured GPP, $GPP_{modelled,i}$ the model result, ε_i the error term and i the interval. The error term is expected to contain serial auto-correlation, so that p-values may be underestimated.

A perfect GPP model would produce only points on the 1:1 line. However, all of the site-EVI-combinations showed strong deviations from that line (Figure 4.5). Although the model results matched the ranges of measurements, which shows that the model works physically reasonable, they overestimated GPP at BR-Ban and BR-Ma2. This is also true when all sites were considered together. The mean for overall $GPP_{measured}$ was 7.849 $g\,C\,\mu mol\,PAR^{-1}$, $GPP_{modelled}$ for the NBAR version was 9.086 $g\,C\,\mu mol\,PAR^{-1}$ and that for the BRDF-adjusted version was 8.764 $g\,C\,\mu mol\,PAR^{-1}$. Both overall VPM results were significantly different from the measurements ($p < 0.01$) as determined by paired t-tests.

BR-Ban, BR-Cax and BR-Sa1 results showed significant correlations ($p < 0.05$) for both EVI versions with GPP, while BR-Ji2 and BR-Ma2 results did not. There seemed to be no spatial pattern behind this distribution, since significant trends appeared both at sites in the deep tropics (BR-Cax) and at the southern Amazon borders (BR-Ban). The overall model performance was very poor: at all sites less than 15% of the variance in $GPP_{measured}$ could be explained by the model results. Additionally, there seemed to be no convincing differences in performance between models driven by NBAR and BRDF-adjusted EVI. This was also true, for another version of VPM, which is supposed to be more useful at semi-seasonal sites

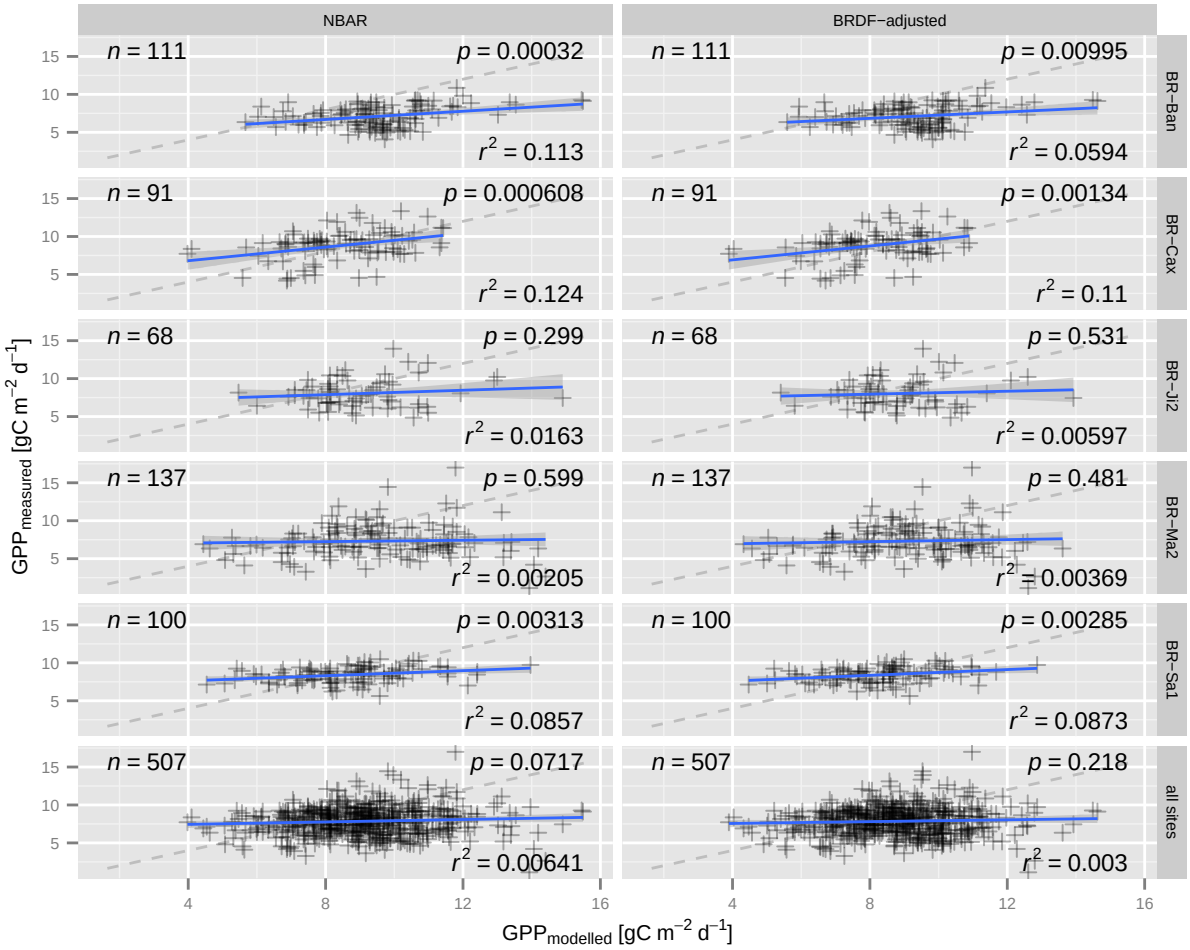

Figure 4.5: Performance of the Vegetation Photosynthesis Model (Xiao et al., 2005) driven by NBAR and BRDF-adjusted EVI at five fluxtower sites, EVI based on level 4 quality filtering (see Table 2.1), blue lines are linear regression models, shaded areas are confidence intervals for regression lines, dashed lines are 1:1 lines, explanations for fluxtowers abbreviations can be found in Table 2.2

like BR-Ban (Figure A.3). Also using EVI as a direct predictor of GPP did not reveal strong differences between the EVI versions (Figure A.4).

Time series of NBAR and BRDF-adjusted EVI, leaf flush and SZA at local solar noon from two forest plots are presented in Figure 4.6. The two sites are situated in different regions of the Amazon basin: While Cax A lies close to the Amazon delta, Tam 6 is situated at the south-western borders close to the Andean foothills (Figure 3.1). Tam 6 provided the longest record of phenological observations.

Cax A did not show strong seasonal patterns in leaf flush. At Tam 6 stronger leaf flush occurred during or at the end of the dry season (JAS), although there was also year to year variation. NBAR and BRDF-adjusted EVI followed very similar patterns at both sites. BRDF-adjusted EVI was generally lower than NBAR EVI. At Cax A, two peaks in EVI occurred during the year: a stronger one at the middle to the end of the dry season and a smaller peak just after the turn of the year. At Tam 6, a more dominant peak at the start of the wet season

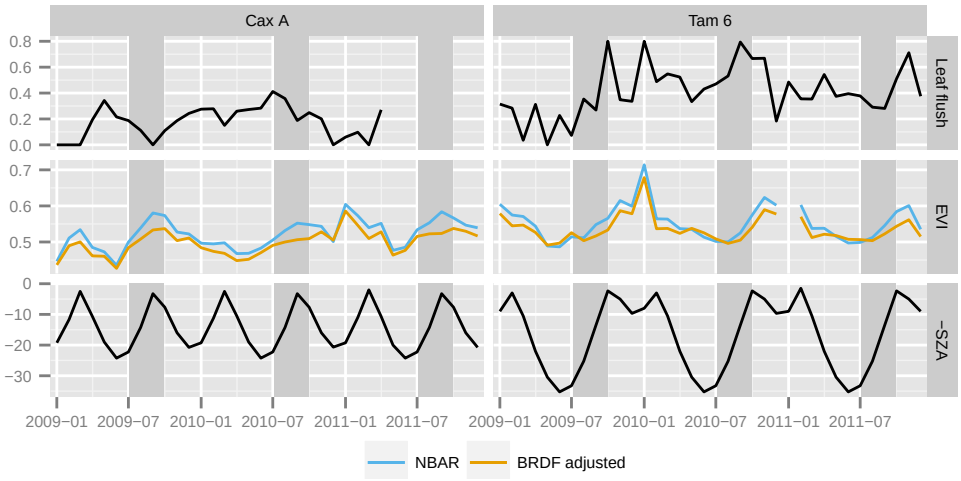

Figure 4.6: Monthly time series of NBAR and BRDF-adjusted EVI, leaf flush and SZA at local solar noon at two forest plot sites, solar zenith angles are reversed to facilitate comparison with vegetation index trends, leaf flush in Mg C $ha^{-1}month^{-1}$, EVI unitless, SZA in degrees, grey bands indicate typical dry seasons (July to September)

dominated the temporal EVI signal. Timing of SZA peaks were according to the positioning to the equator: half a year apart for Cax A, which is close to the equator, and two peaks following close on each other for Tam 6, which is closer to the southern tropic than to the equator. For both sites, the SZA increased during the dry season and peaked shortly before or at the end of it.

Comparing the synchronicity of all lines, EVI seemed to follow SZA much closer than leaf flush. Especially at Tam 6 the one peak pattern over the year can be found in both curves. However, EVI at Cax A clearly showed the first peak during JAS, but the second peak after the turn of the year was not clear in EVI in all years.

Table 4.1 summarizes multiple linear regression models that modelled the influence of leaf flush and SZA on NBAR and BRDF-adjusted EVI at all ground sites. Leaf flush had no significant influence on both EVI versions at all ground sites. Significance levels did not show a particular pattern between NBAR and BRDF-adjusted EVI. On the other hand, SZA had a highly significant ($p < 0.01$) impact on both NBAR and BRDF-adjusted EVI at the Kenia and Tambopata sites. This relationship was still significant ($p < 0.1$) at the Caxiuanã sites for

Table 4.1: Summaries for multiple linear regression models for contribution of SZA at local solar noon and leaf flush dynamics to BRDF EVI

Site	NBAR			BRDF			n
	p leaf flush	p SZA	R^2_{adj}	p leaf flush	p SZA	R^2_{adj}	
Cax A	0.432	0.042	0.175	0.265	0.389	0.048	28
Cax B	0.986	0.086	0.047	0.863	0.570	-0.062	28
Ken A	0.517	< 0.001	0.825	0.353	< 0.001	0.733	20
Ken B	0.882	< 0.001	0.821	0.980	< 0.001	0.718	20
Tam 5	0.740	< 0.001	0.560	0.905	< 0.001	0.284	35
Tam 6	0.422	< 0.001	0.568	0.524	0.002	0.293	35

NBAR processed EVI, but not significant for BRDF-adjusted EVI. Since the SZA is an input to the NBAR processing, the NBAR EVI dependence on SZA is higher. Due to that reason the model could generally explain more variance for the NBAR EVI, which is expressed by higher values of R^2_{adj}. The model performed best at the Kenia sites, acceptable at the Tambopata sites and only poor at the Caxiuanã sites. This depicts the north-south trend in the sites, with Caxiuanã close to the equator. A negative R^2_{adj} for Cax B with BRDF-adjusted EVI points to the fact, that a linear statistical model may not be appropriate for the relationship.

For all models, as for the other linear models in this reports, serial auto-correlation should reduce the p-value for the relationships. However, the influence of SZA on EVI should still be high at the Kenia and Tambopata site, which is supported by the time series plots (Figure 4.6). At the Caxiuanã sites SZA had a significant impact ($p < 0.1$) only for NBAR processed EVI.

4.4 Impact of water stress on dry season greenness

The results of the pixel- and tile-based linear regression models for BRDF-adjusted EVI anomalies and SPI can be seen in Figure 4.7. Figure 4.7a shows the pixel-based approach, with the map of the slope parameter β_1 (Eq. 3.11) on the left and the map for its p-value on the right. Positive values for the slope mean that the EVI responded positive to higher SPI, negative values that EVI decreased with higher SPI. Figure 4.7b presents scatterplots that involved all available EVI–SPI pairs in a tile. They are tiled to represent the spatial orientation of the real MODIS tiles from h10v08 in the NW to h13v10 in the SE. Tile h13v09 covered only one valid forested pixel and tiles h13v08 and h13v10 did not contain any. Positive SPI values mean wetter, negative values dryer than usual conditions.

A cluster of positive responses of EVI anomalies to SPI could be found over western Amazonia. This implies that EVI was low during relative droughts, which supports greenness sensitivity to drought. Some of these pixel-based regressions were statistically significant ($p < 0.1$). Other positive responding regions were located at the Andean foothills in the South, but no significant relationships could be found for them. This was also true for smaller patches of negative relationships in the eastern basin. Otherwise no broad scale spatial patterns could be identified. The relationship was rather patchy with high variation on short ranges. This means that the relationships were random in most of Amazonia.

A curious observation were the p-values themselves: The total number of significant cells at the 0.05 level was 4.1% of all valid pixels. The histogram of p-values for whole Amazonia showed a nearly uniform distribution. This points to a random process that produced significant results only by chance. Additionally, pixels with significant trends were spatially randomly distributed. This speaks against a general relationship between BRDF-adjusted EVI anomalies and SPI.

In contrast to the pixel-based regression modelling, the tile-based approach used statistically more powerful models with more point pairs. All point clouds were clustered at the point of origin for the respective scatterplots. This is typical for anomalies, as the observations are distributed around the overall mean. For tiles h11v08, h11v09 and h13v09 the null-hypothesis of no correlation between SPI and EVI anomalies could not be rejected ($p > 0.2$). In all other tiles the relationships were significant ($p < 0.05$), partially even highly significant ($p < 0.01$). However, all models had very shallow slopes and explained less than 5% of the variance in EVI. This shows that these models are not meaningful in this context. The high number of used points produced significant estimations, which only means that the regression lines are

unlikely to be 0. However, they do not have practical implications to predict the EVI anomaly, which is expressed by the low values of r^2. In this way the tile-based support the findings of the pixel-based approach of no meaningful relation between BRDF-adjusted EVI and SPI.

Figure 4.8 is the counterpart of Figure 4.7 on the basis of the MCWD. Other than in Figure 4.7a, distinct spatial patterns could be found for the EVI–MCWD relationship (Figure 4.8a). Slope parameters close to 0 dominated eastern and southern Amazonia, indicating low predictive power of MCWD for EVI anomalies. North-western regions showed a mixture of both strong positive and negative slopes. This would indicate that EVI anomalies vary with MCWD, which indicates drought impact on canopy greenness. However, in most of these areas the regression slopes were not significant, questioning the value of the relationships. After examining scatterplots for single pixels from these areas, it was clear that these steep slopes were mostly produced by single relatively high MCWD values. Relative in the sense that they were still much lower than maximum MCWD values from other regions, in the order of up to 50 mm. Additionally, pairs with low MCWD values were mostly missing in these cases, possibly due to high cloud cover. This combination led to randomly high or low slope values. The same was true for a strip along the foothills of the Andes at the western edge of the study area, where orographic cloud formation throughout the year hampers good quality observations (Figure 4.1).

As the scatterplots for SPI (Figure 4.7b), the scatterplots for the tile-based approach showed the main characteristic of MCWD (Figure 4.8b): Values clustered at a certain lower threshold. This is 0 for regions that did not experience notable dry seasons in terms of absolute water deficit (h11v09, h12v09). In tile h12v10 values only started at about 100 mm pointing to distinct dry seasons in this area. Independent from that, all point clouds were approximately equally distributed around the 0 EVI anomaly line. In all plots except h12v10 a point of high density towards the lower end of the MCWD axis was observed. Most regression models showed significant relationships of MCWD with EVI anomaly ($p < 0.05$). However, as for the SPI approach, most models explained less than 5% of the variance in EVI. This points to the fact that these models are not meaningful in this context. One exception from that was tile h12v10. Although the explanatory value of the regression was still low, a general negative tendency was observable.

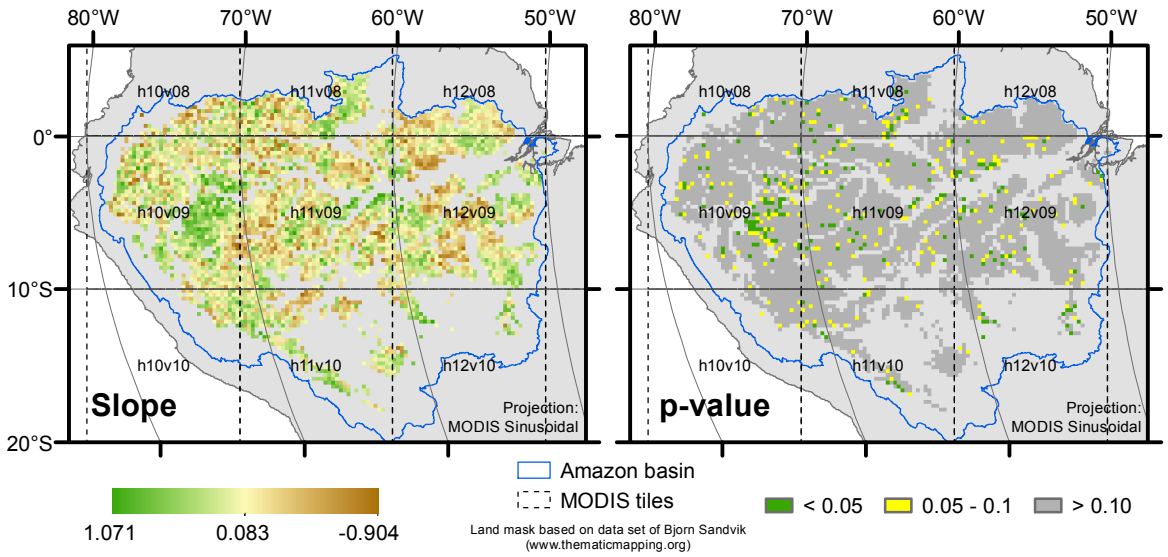

(a) Pixel-based linear regressions on 30 km (~0.25°) spatial resolution

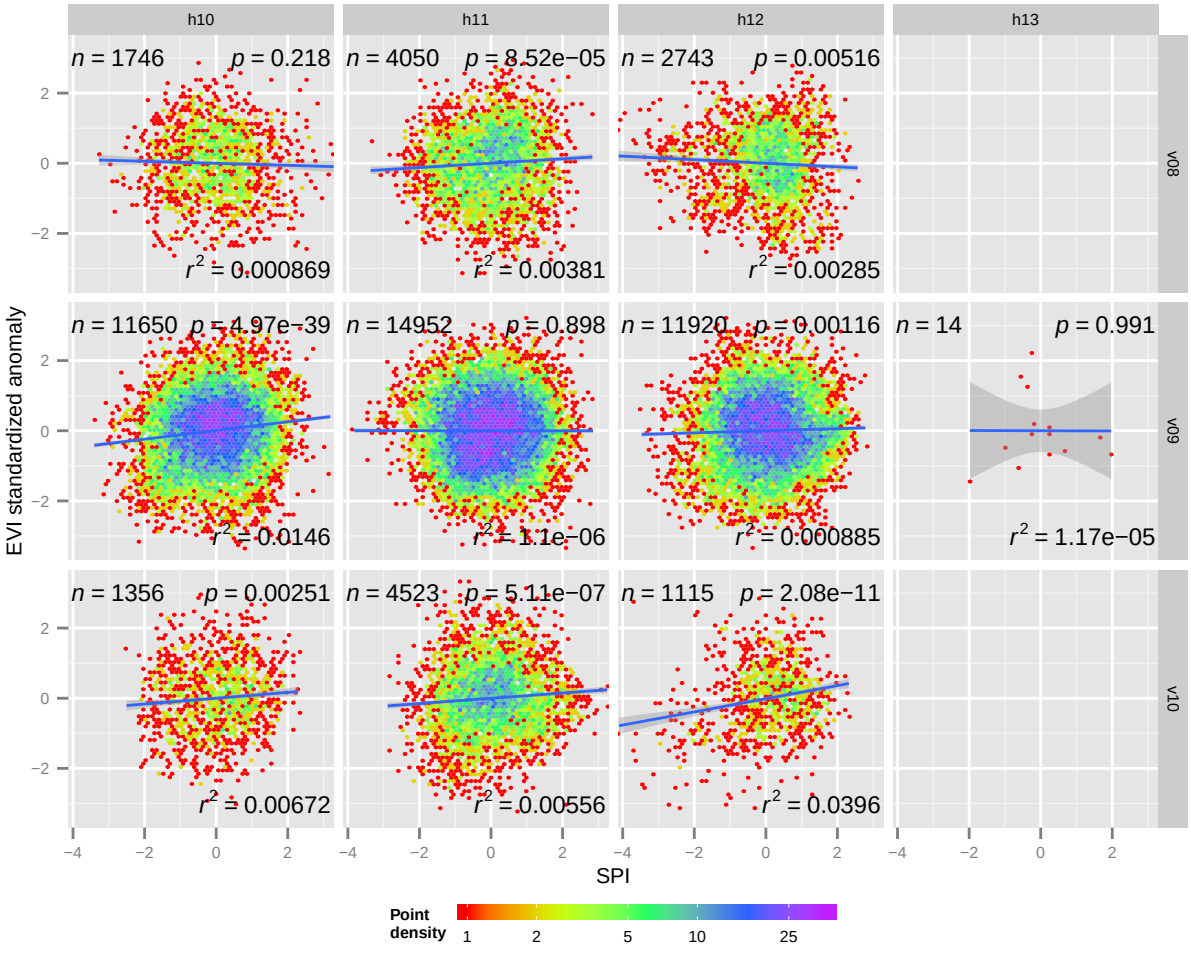

(b) Tile-based scatterplots and regressions, EVI anomalies and SPI dimensionless, plot grid pattern hints at spatial distribution of MODIS tiles, blue lines are linear regression models, numbers are characteristics of linear models per tile, shaded areas are 95%-confidence intervals for regression lines, note that density colour scale is logarithmic

Figure 4.7: Response of September BRDF-adjusted EVI seasonal anomaly to SPI

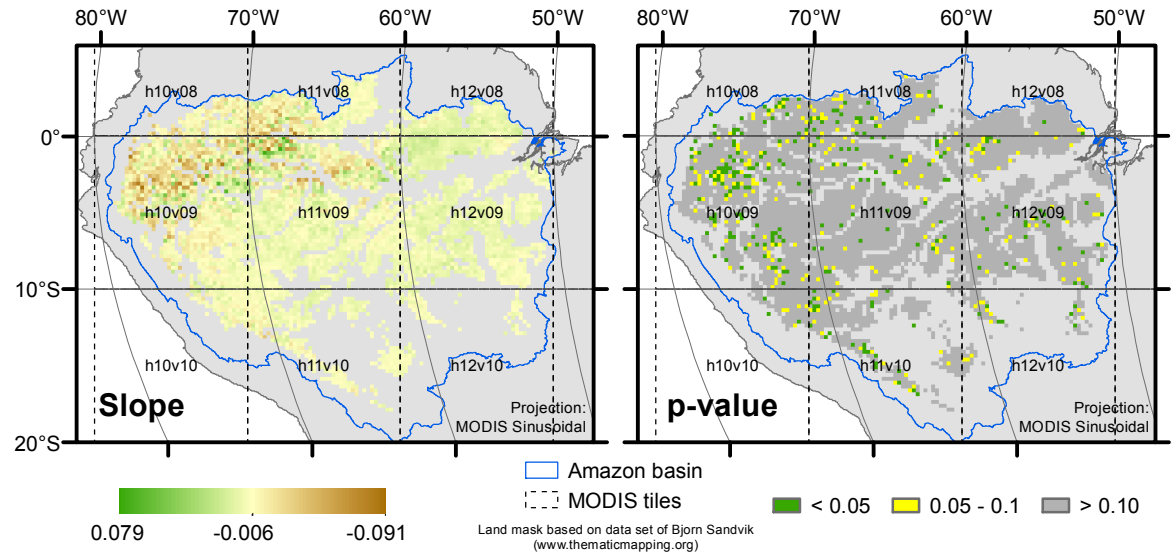

(a) Pixel-based linear regressions on 30 km (~0.25°) spatial resolution

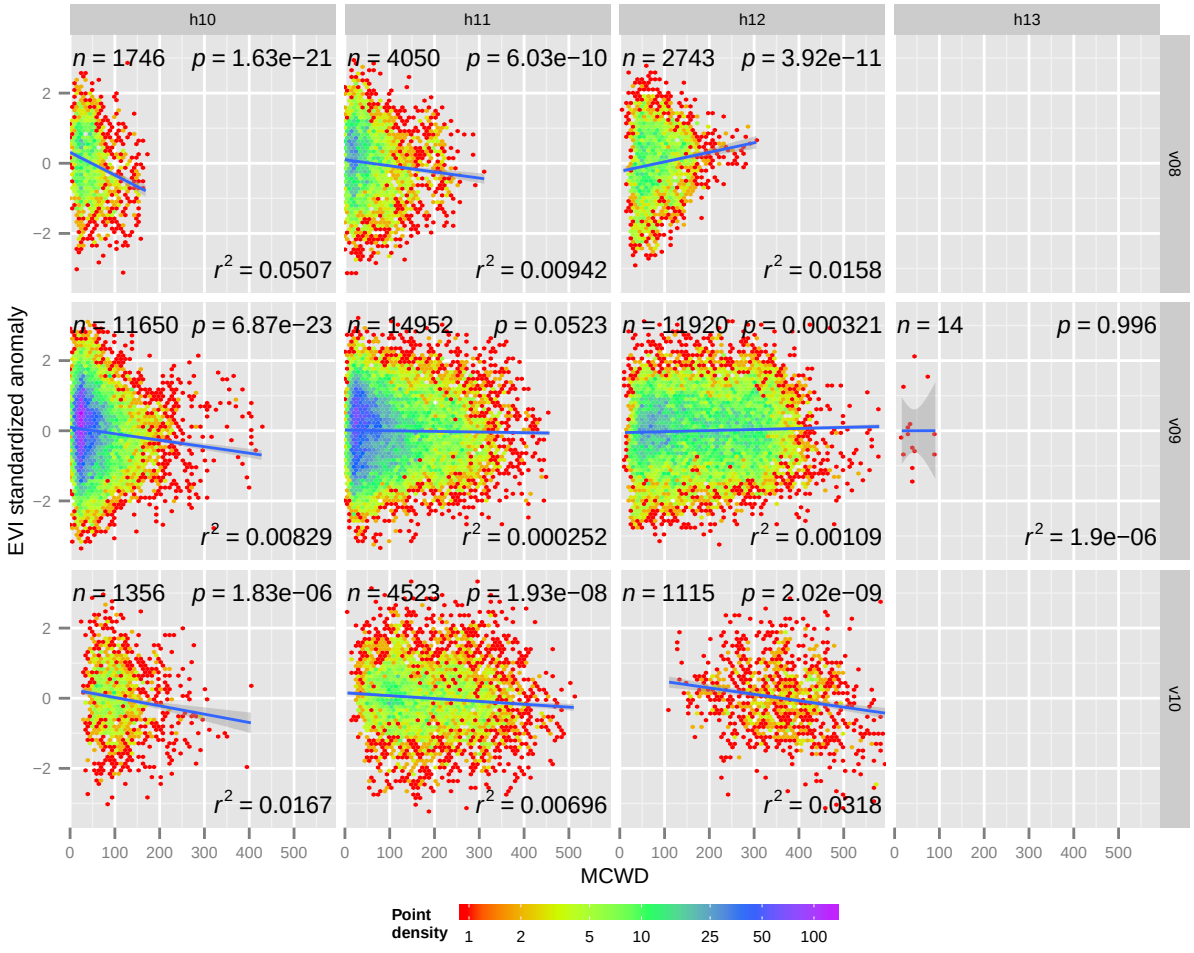

(b) Tile-based scatterplots and regressions, EVI anomalies dimensionless, MCWD in mm, plot grid pattern hints at spatial distribution of MODIS tiles, blue lines are linear regression models, numbers are characteristics of linear models per tile, shaded areas are 95%-confidence intervals for regression lines, note that density colour scale is logarithmic

Figure 4.8: Response of September BRDF-adjusted EVI seasonal anomaly to MCWD

5 Discussion

In this study, I investigated the performance of EVI to study inner-annual dry season and drought impacts on the canopy of undisturbed Amazon forests. I focused on recently discussed SSGEs, which contaminate the temporal EVI signals. Correcting for these effects with the MODIS MCD43A1 product, I found distinct seasonal dynamics of EVI. However, these patterns were suspiciously correlated to SZA patterns over the course of the year on both coarse and fine spatial scales. Furthermore, EVI as part of a carbon uptake model failed to predict GPP at 5 fluxtower locations distributed over the Amazon. This was irrespective of the fact that EVI was corrected for the combined effects of sun and viewing angles (BRDF-adjusted EVI) or for the latter alone (NBAR EVI). Parallel to this, there were no significant relationships between EVI and leaf flush measured at forest plots. Finally, EVI was not sensitive to canopy moisture stress represented by two moisture stress indices, although droughts have the potential to alter forest canopy functioning (Brando et al., 2008) and structure (Phillips et al., 2010).

The following chapter discusses how relevant these results are in context of advantages and disadvantages of the employed methodologies. As Chapter 3 and 4, the discussion follows the order of the research questions. Each section will be closed with a short summary that highlights the major points of the respective discussion.

5.1 Seasonal changes in canopy greenness and structure

To assess coarse scale greenness trends, I reproduced the methodology of Morton et al. (2014) based on an independent BRDF modelling approach. This was possible with the MODIS MCD43 standard product. Particularly, I adjusted EVI to the same sun-sensor geometry on a pixel by pixel basis, thereby focusing on canopy greenness changes and excluding SSGEs. Nonetheless, while Morton et al. (2014) could hardly find any change in the EVI signal throughout the dry season (July to September), the MCD43 BRDF-adjusted EVI showed distinct increases. Although the seasonal amplitudes were strongly reduced compared to NBAR EVI, which is not corrected for SZA-effects, seasonal swings were observable in nearly all recorded years. Of course, the crux of the matter is why these differences occur and which approach characterises real changes in canopy spectral properties better. In this sense it is necessary to take a close look into the differences in methodologies to find possible reasons for deviations.

First, Morton et al. (2014) applied a two band version of EVI leaving out the blue band. In this study, I used the regular EVI based on three bands (Eq. 3.2). Jiang et al. (2008), who introduced the two band EVI, emphasized its high correlation to the three band version. Moreover, EVI is mainly functionally dependent the NIR reflectance (Glenn et al., 2008). Thus using the two band instead of the three band EVI did most likely not result in completely different seasonal patterns.

Second, Morton et al. (2014) defined a slightly different study area. As in this study, they chose MODIS tiles h11v09 and h12v09 as their basis, but focused on Ice, Cloud and land Elevation satellite (ICESat) footprints within the tiles. However, these footprints were spatially well distributed over the two tiles. In this way, the spatial samples should not be strongly

biased, when compared to all h11v09 and h12v09 forested pixels. Thus, the temporal patterns' deviations due to this reason should be small.

Third, Morton et al. (2014) based their landcover masking within footprints on simple thresholds to mask out non-forested pixels. This might have led to deviations compared to the masking in this study, but probably not major differences. Tiles h11v09 and h12v09 represent mostly deep tropical forest, so that random masking errors should generally not result in observations of totally different landcovers. In the end, their derived slopes for uncorrected EVI were comparable to that found here (Figure 4.3). This points rather to differences in BRDF modelling than in spatial subsetting.

And in this respect there is a difference between the methods: Morton et al. (2014) used monthly time slots for their BRDF model inversions, while the MCD43 standard products use 16 day aggregation periods. De Abelleyra and Verón (2014) investigated among other factors the influence of the aggregation period's length on noise in NDVI time series for annual crop fields in the Argentinian Pampas. They defined noise as short term variability in the time series. They found that 16 day periods reduced the noise more than longer periods. The transferability of these results to this study's context might be questionable. But taking into account possible rapid changes in optical canopy properties due to leaf flush, at least some parts of the Amazon forests are comparable to crop phenology. BRDF inversion methods as used by Morton et al. (2014) and in the MCD43 standard products assume stable surface reflectance during the time of data acquisition. This could be violated in case of monthly periods when leaf flush occurs rapidly. Fast leaf production is supported by Figure 4.6 and Doughty and Goulden (2008). In this case the changes in reflectance magnitude are assigned to the changing SZA over the same time in the BRDF inversion process. Thus, the SZA effect might be overestimated in Morton et al. (2014), which provides an explanation for the flat curve in BRDF-adjusted EVI compared to uncorrected EVI.

Inconsistencies between the two results lead to question the BRDF modelling process in general. First of all, this type of aggregation is much more complicated than for instance maximum value compositing. In this type of compositing negative outliers are simply left out. These may be produced by haze and residual clouds, which were not detected in the quality screening. BRDF modelling on the other hand depends on all available observations. Although Lucht et al. (2000a) point out that "... [if] the inputs [of the BRDF-modelling process] had a random component of, for example, 10% magnitude, the albedos retrieved would only vary by about 2–5%". But this is valid for albedos, i. e. the integrals over the sun and/or observational sphere. Single BRFs might carry higher errors. Moreover, clouds introduce a directional – not a random – component into the modelling process. Clouds and aerosols also follow seasonal patterns with high cloud cover during the wet season and high aerosol loads during the dry season due to biomass burning. This seasonality might propagate into the final temporal greenness patterns.

Another factor influencing the BRDF modelling process is the spatial accuracy of gridded MODIS products. With an average overlap of observation and grid of less than 30% (Tan et al., 2006), observations only partially consist of the signal of the grid cell. Since the modelling process integrates all available observations, it is sensitive to these artifacts. What can possibly counterbalance these inaccuracies are spatially homogenous canopies. If neighboring forests react equally to environmental conditions, their BRDF properties will be similar and the error introduced due to spatial mismatch limited. Systematic studies have not addressed this relationship in respect to BRDF modelling yet.

Table 5.1: RTLSR model parameters and their coefficients of determination for forests as found in the literature and this study, parameters for this study are spatio-temporal averages for MODIS tiles h11v09 and h12v09

Forest type	visible/red				NIR			
	f_{iso}	f_{vol}	f_{geo}	R^2	f_{iso}	f_{vol}	f_{geo}	R^2
Pineforest (Roujean et al., 1992)	0.037	0.133	0.000*	0.50	0.282	0.243	0.017	0.15
Temperate, broadleaf, deciduous (Roujean et al., 1992)	0.030	0.087	0.000*	0.52	0.400	0.295	0.040	0.32
Tropical, broadleaf, evergreen (this study)	0.036	0.039	0.008	–**	0.371	0.214	0.073	–**

*Parameters have been set to 0 after retrieval of negative (unphysical) values.
**MCD43 product does not provide this information.

Given these uncertainties in the general modelling process, I screened the literature for values of RTLSR model parameters f_{iso}, f_{vol} and f_{geo} derived with more certainty. Unfortunately, not many studies present the actual parameter values. Table 5.1 presents the parameters derived in this and one other study. The values for this study correspond to the RTLSR parameters that led to the contributions of the three model terms in Figure 4.4 averaged over the whole study period. Overall, the individual parameters had the same orders of magnitude across the studies. Also for all studies NIR parameters were larger than those for the visible/red spectrum, which follows the typical relationship for reflectances of vegetation. However, geometric scattering played a larger role in this study. This might be explained by stronger shadowing within tropical forests. Large trees cut gaps into the canopy when they fall, which causes shadowing effects. Also single emerged trees make the canopy more heterogeneous and cast shadows. Even though the parameters were derived on much different spatial and temporal scales, the comparison shows that MCD43 parameters were in general agreement with those found for other forested surfaces.

However, as in all statistical fitting procedures there are measures for the quality of model fits, mostly expressed as the coefficient of determination R^2. This is also true for statistical BRDF inversions. Table 5.1 contains these coefficients, which Roujean et al. (1992) obtained from their fitting. While R^2 was acceptable for other vegetation covers in the study of Roujean et al. (1992) – typically above 0.8 – forests posed problems to the kernels. Especially in the NIR the fit was rather poor, with only 32% explained variation for a broadleaf forest. Hu et al. (1997) even applied a whole ensemble of kernel combinations including the RossThick and LiSparse kernels on the same data set as Roujean et al. (1992). They arrived at a comparable fit in the NIR. Even though both studies were based on only one data set (Kimes et al., 1986), these findings could indicate problems of the RTLSR to capture variations in the BRDF of forests. Figure 2 of Hu et al. (1997) offers a possible explanation for this: While the fitted RossThick-LiSparse and RossThin-LiSparse models have particular hot spots, the observations did not show a hot spot. This is supported by the findings of Bréon et al. (2002). Using the Polarization and Directionality of Earth Reflectances (POLDER) instrument with its high angular resolution, they found only low hot spot amplitudes for evergreen broadleaf forests compared to other landcover types. This means that the semi-empirical models might not

represent the BRDF well. This shortcoming would apply for both this and the study of Morton et al. (2014).

Furthermore, results presented in Figure 4.4 raise concerns about the performance of the BRDF modelling with the MCD43 standard product. Although correlations between EVI and SZA were strongly reduced after correcting for BRDF, some plot site analyses showed only minor changes in EVI after correction and high correlation with the SZA (Figure 4.6). On the first sight, this might support the hypothesis of light limited Amazon forests, so that the forests make use of the increased radiation (Myneni et al., 2007). On the other hand, it is peculiar that BRDF-adjusted EVI did not only increase during the first sun nadir positioning at the end of September, but also at the second in March (Figure 4.3). The second nadir position is in the midst of the wet season, when cloud cover strongly blocks solar radiation. For that point in time the hypothesis of light limitation is not valid. In this sense it is more likely that the BRDF modelling did not fully account for SSGEs.

Leaving EVI aside, it is also interesting to take a glance on NDVI. NDVI did not show strong changes after correction for SSGEs (Figure 4.3). This means it is more robust against these effects. This is due to its formulation as a ratio; BRDF effects cancels out, because they are similar in the red and NIR bands (Vermote et al., 2009; de Abelleyra and Verón, 2014). Figure 5.1 illustrates this property. The graphs are based on RTLSR parameter values derived from BRDF tiles h11v09 and h12v09 averaged over time. These values are listed in Table 5.1. The three dimensional graphs show the BRDFs shapes of NDVI and EVI2. EVI2 is the EVI version used by Morton et al. (2014). It does not incorporate the blue band, but is highly correlated with EVI (Jiang et al., 2008). It is formulated as:

$$EVI2 = 2.5 \times \frac{\rho_{NIR} - \rho_{red}}{\rho_{NIR} + 2.4\,\rho_{red} + 1} \tag{5.1}$$

The horizontal axes represent viewing zenith angles in the principal and cross-principal planes. They might be misleading, because they are only valid for these two planes. In fact, the distance from the point of origin marks the real viewing angles. The vertical axes represent the vegetation index value. The NDVI BRDF resembles a plateau, indicating its resilience against sun-sensor geometry over a wider range of angles: When the SZA stays constant and one moves away from the point of origin, the index stays almost constant. This is very different for EVI2. Only slightly changing the VZA, changes the vegetation index a lot. This is true for both SZA 10° and 30°. Now changing the SZA and keeping the VZA constant also changes the resulting vegetation index a lot.

Despite this positive characteristic of NDVI, it mostly saturated in this study. This was one major reason why it was replaced by EVI for dense vegetation canopies (Huete et al., 2002). Additionally, NDVI showed opposite seasonal patterns than would be expected from leaf flush. This is NDVI decreased during the dry season.

All in all, the results of this study do not support the hypothesis of stable greenness patterns as proposed by Morton et al. (2014). Instead, EVI was distinctly higher during the wet season compared to the dry season. I see the major reason for these discrepancies in the different aggregation periods of the methods. As both methods assume stable reflectances over the modelling period, the longer interval of Morton et al. (2014) might miss subinterval greenness changes. However, MCD43 BRDFs-adjusted EVI was still highly correlated with the SZA. A small literature survey revealed possible problems of the RTLSR model to reproduce the BRDF for broadleaf forests, especially in the NIR.

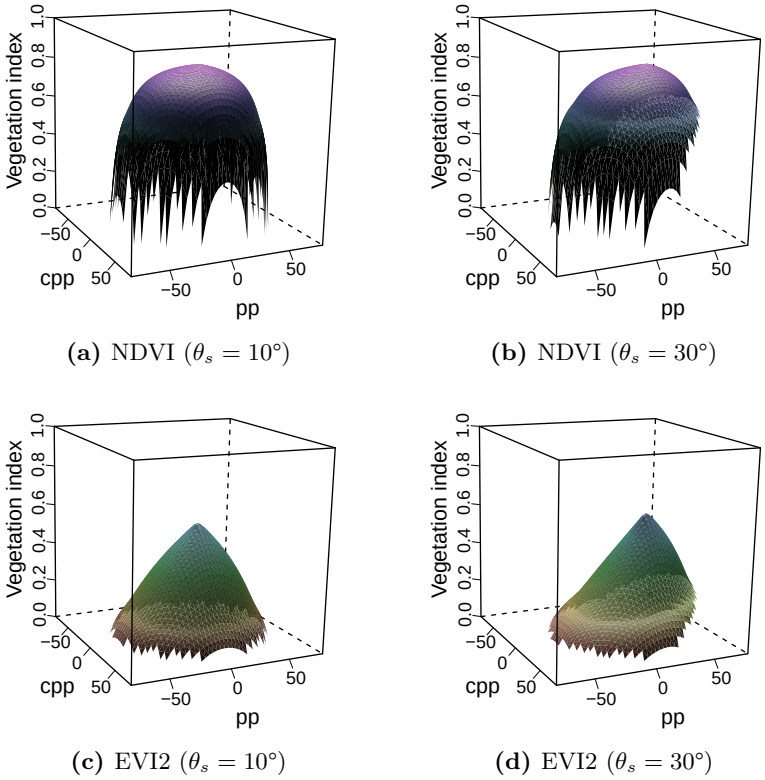

(a) NDVI ($\theta_s = 10°$) **(b)** NDVI ($\theta_s = 30°$)

(c) EVI2 ($\theta_s = 10°$) **(d)** EVI2 ($\theta_s = 30°$)

Figure 5.1: NDVI (top) and EVI2 (bottom) Bidirectional Reflectance Distribution Functions (BRDFs) for solar zenith angles 10° and 30°, horizontal axes represent viewing zenith angles in the principal (pp, $\phi = 0°$ and $\phi = 180°$) and cross-principal plane (cpp, $\phi = 90°$), color and shade to facilitate 3D illustration

5.2 Relationship of canopy greenness to carbon uptake and phenology

Besides the question of seasonal changes in canopy greenness expressed as EVI, it is important how greenness is actually coupled to canopy processes and properties. In fact, this relationship lays the foundation for the discussion of SSGEs (Section 5.1): the strength of the relationship determines how serious greenness should be taken for the health assessment of Amazon forests. EVI is commonly treated as a proxy for photosynthetic activity and carbon uptake expressed as GPP (Brando et al., 2010; Xu et al., 2011) or as a mixed effect of canopy structure and functioning (Gao et al., 2000). In contrast to NDVI, EVI does not saturate over high biomass forests such as the Amazon forests (Huete et al., 2002), and is therefore preferably applied to investigate Amazon phenology (Saleska et al., 2007).

On the other hand, EVI validation studies, which focus on evergreen tropical forests, are rare. Screening through EVI review studies like Huete et al. (2011), it becomes evident that validation has concentrated on temperate forests. Well equipped fluxtower networks like Ameriflux make it much easier to conduct meaningful validation in temperate than in tropical forests (Rahman et al., 2005; Sims et al., 2006). Actually, Xiao et al. (2005) offer a validation approach for

the BR-Sa1 fluxtower by adapting the VPM to a tropical site for the first time (Eq. 3.3). Unfortunately, they did not directly compare their results to eddy covariance measurements.

The validation for the EVI–GPP relationship provided in this study points to a potentially critical overestimation of the EVI's predictive power. As part of the remote sensing based carbon uptake model VPM, EVI failed to predict major variability in GPP (Figure 4.5). Also using a modified model formulation or EVI as a direct predictor for GPP did not improve the relationship (Figure A.3, Figure A.4). These results are particularly important, because the involved fluxtowers are distributed over most of Amazonia, representing different environmental conditions. Only western Amazonia is not represented (Figure 3.1).

Furthermore, the spatial window used as the remote sensing footprint was comparable with footprints of other studies. Davis et al. (2003) speak about a spatial representativeness of 1 km^2. Investigating a realistic footprint size, Chen et al. (2012) found sizes ranging from 2.55 to 5.04 km^2 at nine Canadian forested sites. They emphasized the footprint's dependence on landcover homogeneity around the tower. This in mind, the BR-Cax, BR-Ma2 and BR-Sa1 towers have very homogenous surroundings consisting of closed canopies. Also BR-Ban is located in a dense forest, but rivers flow in the neighbourhood of both BR-Ban and BR-Ji2. Additionally, agricultural fields are situated west of BR-Ji2. Within the remote sensing processing they are taken care of with the landcover mask. Even though, GPP retrievals can be influenced especially at BR-Ji2, the model performance was not much different at BR-Ban or BR-Ji2 compared to the other sites (Figure 4.5). Thus, the footprint size seemed to have no major impact on the inter-comparison of remote sensing and tower based data.

On the other hand, the translation of EVI into GPP depends on the quality of the VPM's theoretical framework. In recent years the development of carbon uptake models supported by remotely sensed vegetation indices has been pushed forward. However, no consensus about a best approach has been found yet (Hashimoto et al., 2012). Earlier models used NDVI to approximate $FAPAR_{PAV}$ (Running et al., 2004). With MODIS images coming available in 2000, EVI has been used more and more for high biomass ecosystems, for example in the VPM (Eq. 3.4). In some studies direct comparisons of EVI and GPP showed lower predictive power of EVI for evergreen versus deciduous (Sims et al., 2006; Hashimoto et al., 2012) and for tropical versus non-tropical sites (Hashimoto et al., 2012). Against this background the low performance of VPM with both NBAR and BRDF-adjusted EVI in this study is in line with the literature.

Still the question remains why. Sims et al. (2006) discuss the need for an independent estimate of LUE complementing EVI as an estimate for $FAPAR_{PAV}$ to improve model performance for evergreen sites. LUE in VPM is actually such a term (Eq. 3.4), but explanatory power of the VPM was even lower here than solely using EVI (Figure 4.5, Figure A.4).

Furthermore, the VPM expresses water stress in the water scalar (Eq. 3.8), which makes use of the LSWI (Eq. 3.7). Biudes et al. (2014) analysed seasonal dynamics of LSWI at a semi-deciduous tropical forest and found strong negative correlations with water availability measures such as rainfall, soil water content and relative humidity. They point out that new, young leaves, which grow in the dry season, have a higher leaf water content, thus increasing the water sensitive LSWI. This argumentation might also be applicable to evergreen sites, if they experience large scale leaf flush. In this way new leaves may have a higher LSWI during the dry season compared to the wet season. The formulation of the water scalar (Eq. 3.8) would then imply that the canopy suffers from water stress during the wet season, which is certainly not the case. Apart from that, SSGEs could also affect LSWI, as it is based on NIR reflectance (Eq. 3.7). NIR reflectance appeared to be strongly affected by directional effects (Figure 4.3). This would produce artificial seasonality that does not need to be related to canopy water

stress. Finally, the discussion if Amazon forests are light or water limited has not settled yet (Morton et al., 2014). Thus the question if and how water stress needs to be dealt with in carbon uptake models for tropical forests remains open.

Another problem in the analysis is the availability of remote sensing data. As presented in Section 4.1, the wet seasons strongly reduce good quality the satellite observations. This affects the statistical evaluation. Thinking of the scenario that the wet season retrievals produce higher GPP estimates, they would stretch the point clouds in Figure 4.5. In this way the analysis is temporally biased.

Furthermore, residual clouds, atmospheric conditions, differences in surface moisture, and geolocation errors challenge the robustness of the BRDF inversion process (Lucht et al., 2000a). Even during the dry season up to 66% of all observations can be contaminated due to aerosols (Samanta et al., 2012b). Although Lucht et al. (2000a) state that the BRDF modelling process is relatively robust against random noise, directional noise might affect the reflectance estimates and hence EVI. In contrast to the analysis of seasonal EVI patterns (Section 3.3), the GPP modelling depends on the actual magnitude of EVI. This is because GPP is a linear function of EVI in the VPM (Eq. 3.3), so EVI magnitude changes will directly translate into GPP estimate changes. These directional changes might explain the general GPP overestimation of the VPM (Figure 4.5).

Both of these problems – missing observations and possible contamination – also apply for the leaf flush related analysis. As argued before due to missing data during the wet season the linear regression models might have performed worse than if data from the whole year would be available. Nonetheless, leaf phenology in the data used here was much different compared to published patterns. The leaf flush time series here (Figure 4.6) missed seasonal cycles as strong and regular as remote sensing studies proposed (e. g. Samanta et al., 2012c; Myneni et al., 2007). This stemmed from the method and data for the derivation of leaf flush. Leaf flush was defined as the change in detected leaf mass corrected for the litter fall mass. While the litterfall followed seasonal cycles, LAI was rather stable and more dominated by inter-annual trends (graphs not shown). The resulting leaf flush blended these patterns into time series with fewer regular characteristics. On the other hand, Brando et al. (2010) found more regular patterns of leaf flush. Their method differed from the one used here: they counted the number of trees in forest plots with new leaves This approach may introduce some subjectivity, since the it was a manual assessment. Standardized measurement protocols for leaf flush have not been established yet. In this sense the results of the leaf flush analysis have to be treated carefully.

As in the coarse scale seasonality assessment, EVI showed peculiar statistical relationships with the SZA for two forest plots sites over the course of the year (Table 4.1). Here, SZA explained much more variability in EVI than the leaf flush signal. In this sense it can be speculated that SSGEs are not properly accounted for during the BRDF modelling process. Relationships between EVI and any ground processes might therefore be rather statistical. This is because seasonal processes are strongly correlated when they have the same frequency and are in phase. The two Caxiuanã plots are an exception from this. BRDF-adjusted EVI was not significantly correlated with the SZA (Table 4.1). This contradicts a simple explanation of EVI as totally depending on SSGE.

In summary, the approach here could not show a relationship between EVI and canopy processes as it was claimed by several studies. However, this conclusion has to be treated carefully. There is no best practice approach to model carbon uptake of tropical forests via remote sensing. Also leaf flush was only recently discovered as a possible important process in Amazon forest phenology and misses a commonly accepted measurement protocol. But if these

results can be taken seriously, the EVI's suitability for assessment of canopy processes has to be evaluated critically.

5.3 Impact of moisture stress on dry season canopy greenness

Anomalies of BRDF-adjusted EVI were generally insensitive to drought expressed as SPI and MCWD. These results have particular significance, because they were derived on both coarse and medium spatial scales. Moreover, they did not only focus on drought years like the 2005 or 2010, but were based on a general assessment over all years when data was available. In this way positive and negative anomalies were assessed in a broader context; chances were lower to interpret spatial or temporal noise in EVI as a response to drought. This can happen if only single drought events are considered for analysis. Furthermore, using seasonal anomalies to analyse EVI sensitivity is robust against seasonal patterns. Anomalies remove seasonal patterns such as viewing and sun geometries and highlight dissimilarities between the years. However, this analysis focused on direct impacts, which occur in the same year as the drought event. Impacts on longer time scales as found by Saatchi et al. (2013) were beyond the scope of this study and cannot be excluded.

A critical point is the definition of the dry season. A number of studies – including this one – simply assumed the three months July, August and September to be the driest period of the year for large areas (e. g. Aragão et al., 2007; Saatchi et al., 2013; Samanta et al., 2010, 2012a,c; Xu et al., 2011; Zhao and Running, 2010). Other definitions employed thresholds like 50 or 100 mm precipitation per month (Anderson, 2012). If a months falls below this threshold it is considered as dry. Marengo et al. (2001) and Fu et al. (2013) apply thresholds combined with moving windows to find dry successional intervals. This accounts better for the idea of the dry season as a continuous period during the year. However, none of these approaches is considered as best practice, so that the choice is made with every study anew. Additionally, none of these approaches explicitly considers the spatial dimension, although all accept the idea of longer dry seasons in southern Amazonia.

In this context, the month September, which I picked to represent the most pronounced part of the dry season, is certainly not the driest month for all Amazonia. Nonetheless, this should be at least the case for some regions. And if greenness expressed as EVI would be sensitive to abnormal dry or wet conditions, these regions should be identifiable. But in both maps (Figure 4.7a, Figure 4.8a) no such regions were clearly visible. In this sense, this parametrisation should not have influenced the conclusion of low correlation between EVI and drought.

In respect to the drought indices themselves, it is important how well they can reproduce the water stress on the canopies. As already mentioned, the discussion around this topic is not settled. Even more, I could not find any study systematically assessing the power of drought indices in the context of tropical forests. However, Li et al. (2008) studied the long-term trend in SPI over the Amazon to assess how drought conditions might develop under different scenarios of climate change. Their argument for the SPI was that it is a flexible index, which adapts to local rainfall regimes. This is because it represents relative droughts, which occur in every system with seasonal rainfall patterns. Only they applied the SPI on 30 year time series. In fact, McKee et al. (1993), who presented the index, recommended to use time series of more than 30 years. Here the time series had only a length of 14 years. This has particular implications for pixels for which the precipitation time series do not present a good sample of the climatological mean. However, the final impact on the results is hard to tell.

Trenberth et al. (2013) point to another critical point of the SPI: it is based on precipitation alone, without considering the forest's demand for water. In this sense, it could be argued that vegetation adopts to average precipitation to optimize growth. From this perspective SPI reproduces drought events well, because it represents the probability of how far away a given time interval is from the mean. If this is extraordinary dry, the canopy should respond to this.

Beside this, MCWD represents an absolute drought index and is affected by the value for evapotranspirational demand. This value is equivalent to the precipitation threshold mentioned above when the focus is on drought impacts on vegetation. But in contrast to the discussion about dry season thresholds, the MCWD evapotranspirational demand is generally accepted as 100 mm month^{-1}. Of course this gives a first approximation, but might leave out considerable spatial variation. For example, some tropcial tree species shed their leaves during the dry season and thus reduce water loss for the whole canopy (Markesteijn and Poorter, 2009). Aragão et al. (2007) argue that MCWD does not incorporate plant adaptations, because these are only poorly understood for Amazon rainforests. The fixed value for the demand might have produced the seemingly heterogeneously responding area in western parts of the Amazon basin (Figure 4.8a). These regions hardly experience dry seasons (Marengo et al., 2001) and the obtained patterns represent rather randomly high or low EVI values when MCWD is occasionally larger. Nonetheless, MCWD proved valuable as a predictor for tree mortality rates in a pan-tropical study (Phillips et al., 2010).

Another point is how water availability is dealt with. Both indices assume a simple bucket model without interactions with neighbouring cells. In this way, through-flow is not considered. Apart from that, some studies argue that some species with deep roots have access to water during the dry season (Nepstad et al., 1994; Poorter and Hayashida-Oliver, 2000). This can protect them from water stress even during prolonged drought. However, these adaptions are only known on plot scales and their spatial distribution has yet to be determined.

Other studies investigating the EVI–drought relationship on coarse scales diverge in their results. Saatchi et al. (2013) analysed satellite-borne radar backscatter and found a clearly defined region in western Amazonia that was affected by the drought of 2005. Backscatter anomalies remained low up to 4 years after the drought event. The EVI–SPI response map (Figure 4.7a) showed a smaller region partially overlapping that of Saatchi et al. (2013), which was sensitive to wet and dry conditions: The slope lines for the regressions were positive there, meaning higher SPI values (wetter conditions) were accompanied by higher EVI values and vice versa. However, this region was substantially smaller than that of Saatchi et al. (2013) and responses elsewhere in the region of Saatchi et al. (2013) were inconsistent. The EVI–MCWD map did not show responses in this region (Figure 4.8a). Overall, the mentioned region in the EVI–SPI response map might follow the pattern in Saatchi et al. (2013), but is not consistent.

Xu et al. (2011) found wide spread negative anomalies over the whole Amazon forests for the drought year 2010 when analyzing MOD13A2 EVI based on images of the Terra MODIS. However, they did not consider a praticular trend in the MOD13A2 data: Wang et al. (2012) found a decrease in NDVI of 0.001–0.004 yr^{-1} due to sensor degradation. The negative trend was larger for Terra than for Aqua MODIS. Since Xu et al. (2011) used Terra MODIS vegetation indices at the end of their defined time series, the chance for retrieving negative anomalies is on average higher than at the start of the time series due to the overall, negative trend. This might have resulted in negative anomalies all over the Amazon basin and lead to the conclusion that the 2010 drought would have had a major impact on vegetation greenness.

This argumentation is supported by the study of Samanta et al. (2010). As Xu et al. (2011), Samanta et al. (2010) made us of MOD13A2 EVI. But they derived anomalies at the middle of

their time series, instead of at the end. In the middle the negative trend should cancel more or less out. Consequently, Samanta et al. (2010) could not find uniform greenning or browning behaviour throughout the Amazon basin in response to the 2005 drought.

Along with the leaf flush and drought impact discussion, the question was raised if Amazon forest productivity is limited by light rather than water supply. Considering the weak responses of EVI to both drought indices, it seems reasonable that the forests do not suffer from moisture stress. However, EVI's weak explanatory power for ground processes in this study questions if canopy greenness expressed as EVI is a good help to answer this question. It is rather the question, what canopy greenness expresses in the context of tropical evergreen forests. Radiative transfer theory and experiences in mid-latitude forests proofed the usefulness especially of the NIR spectrum. Dense canopies may proof a challenge, if NIR reflectance saturates and variations are due to other reasons than water stress.

Altogether, I aimed at finding a general relationship between canopy greenness expressed as EVI and drought expressed by two drought indices. Results for both indices suggest that no such general relationship exists on coarse spatial scales. This is in agreement with other studies that are based on EVI. Main shortcomings of the applied methods concerns the static dry season definition as well as missing validation of the drought indices' performance.

6 Conclusions & recommendations

The Amazon rainforests represent the largest connected forested area in the tropics and play an integral role in the global carbon cycle. In recent years the discussion about their phenology and response to drought has become intense. While some studies found severe drought impacts on tree mortality and canopy structure, others suggested high resilience and even canopy green-up during periods of water deficit. Studies based on remote sensing products and especially the Enhanced Vegetation Index (EVI) explained this by leaf flush during the dry season. Newer studies claim this effect to be an artifact of sun-sensor geometry, which was not considered in previous studies.

In this study, I stressed the performance and plausibility of EVI in three different approaches. In all of them I employed an EVI corrected for SSGEs derived from the MODIS MCD43 product suite. First, I performed a coarse scale comparison of EVI seasonality with a recent study (Morton et al., 2014). Both results differed remarkably pointing to discrepancies in the BRDF modelling approaches. Additionally, the MCD43 BRDF-adjusted EVI showed partially high, unlagged correlations with the SZA. This does not imply a causal relationship, but raises suspicions if the MCD43 BRDF modelling process fully accounts for SSGEs. Second, I conducted a small scale validation for the power of EVI to predict carbon uptake and canopy leaf flush. These results have to be treated carefully as remote sensing driven carbon uptake models are not yet well developed for tropical forests and measurements protocols for leaf flush are not well established. However, if the results can be taken seriously, EVI has difficulties to predict both ground processes. Third, I analysed the relationship between EVI and two drought indices on coarse and medium spatial resolution. EVI anomalies showed no meaningful general relationship with the drought indices.

Nonetheless, a specific region in western Amazonia showed a relationship between relative drought and EVI greenness. This region coincided with a highly drought sensitive region found in a radar-based study. Radar backscatter is sensitive to canopy structure and water content. Also BRDF-adjusted EVI was highly independent from the SZA at the Caxiuanã forest site, though not correlated with leaf flush. Both points raise the question if EVI is rather linked to other canopy processes not tested in this study.

Overall, these results together question the usability of BRDF-corrected EVI based on the MCD43 product suite to assess the functioning and/or structure of tropical forests in the Amazon basin. I agree with Morton et al. (2014) in the point that SSGEs heavily influence EVI. However, I see sufficient evidence from ground-based studies for functional and phenolocial seasons in Amazon forests. This seasonality should impact remote sensing measures of Amazon tropical forests. Regarding EVI, I propose two alternative, speculative scenarios:

- Both BRDF modelling approaches (MCD43 and Morton et al.) incorporate important modelling elements, but fail to completely correct for SSGEs. EVI is generally suitable to detect tropical forest functional and/or structural seasonality, but has to be properly corrected for SSGEs.

- The vegetation greenness concept implemented with EVI in general is not applicable for tropical forests. Evergreen tropical forest canopies prevent the detection of process-based changes.

If the second scenario would apply, it would have serious implications for coarse scale ecological studies employing EVI as a proxy for forest functioning. However, vegetation indices have proven useful for temperate zones with distinct seasonality. Based on radiative transfer theory, reflectances should carry information about the observed vegetation structures. Vegetation indices might just have to be reevaluated under tropical conditions.

During the working process I came across several questions that might be addressed in future research. First of all, I see the need to review the BRDF modelling process for tropical deciduous forests. Morton et al. (2014) surely provoke reactions in this respect. A meaningful point here is the shape of the BRDF, especially in the NIR band. Multi-angular instruments such as POLDER and MISR aboard Terra offer operational, wide spread angular sampling. This could be used to study spatio-temporal behaviour of the tropical canopy BRDFs. Especially the question how strong canopy BRDFs change in respect to reflectance changes is important for the modelling process. Also ground-based sensors should be involved. For instance, fluxtowers offer valuable opportunities, because they emerge from the canopies and provide technical infrastructure for recording and storing data. They might be used as platforms for optical sensors. Also Unmanned Aerial Vehicles (UAVs) may be operated from fluxtowers. They can scan the same part of the canopy at several viewing angles in a short time and repeated over the day to explore reflectance dependence on sun and viewing geometry.

Furthermore, the Fluxnet community announced a new synthesis data set that extends available time series of tower based measures such as GPP. These new capacities should be used to assess the relationship between canopy carbon fluxes and remote sensing measures. Concerning forest plots, I see some applications for another type of field study: Drought experiments were set up to study the forest dynamics under water stress. Irrigation experiments could be set up to answer the question, if forests experience seasonality even without water stress. This could contribute to answer the question if Amazon rainforests are limited by light or water.

Besides broad band spectral indices, the potentials of new approaches based on satellite-borne sensors can be explored to detect seasonality in tropical forest functioning and canopy structure. This is in particular solar-induced chlorophyll fluorescence (Meroni et al., 2009), the Photochemical Reflectance Index (PRI) for LUE estimation (Drolet et al., 2005) and indices based on thermal bands (Caccamo et al., 2011). Especially structural indices are interesting for canopy structural parameters (Chopping, 2008). These are for example the Structural Scattering Index (SSI) (Gao et al., 2003), the Canopy Structural Index (CSI) (Sharma et al., 2013), and the Anisotropic Flat Index (AFX) (Jiao et al., 2014), to name only some. These indices typically evaluate the shape of the BRDF and give information on the surfaces' scattering properties, which depend on canopy structure. Of course, these indices depend on high quality BRDF modelling and need to be validated with ground-based data.

In respect to the detection of dry season and drought, I see potential in the incorporation of evapotranspiration estimates into the determination of water stress. Although evapotranspiration estimates introduce another source of error into the algorithm, this would give a much more realistic approach to detect plant water stress. Apart from that a validation of climatological drought indices in the context of tropical forests is prerequisite for their use.

References

Aide, T. M.: 1993, 'Patterns of leaf development and herbivory in a tropical understory community'. *Ecology* **74**(2), 455.

Anderson, L. O.: 2012, 'Biome-Scale Forest Properties in Amazonia Based on Field and Satellite Observations'. *Remote Sensing* **4**(12), 1245–1271.

Anderson, L. O., Y. Malhi, L. E. O. C. Aragão, R. Ladle, E. Arai, N. Barbier, and O. Phillips: 2010, 'Remote sensing detection of droughts in Amazonian forest canopies'. *The New Phytologist* **187**(3), 733–750.

Aragão, L. E. O. C., Y. Malhi, R. M. Roman-Cuesta, S. Saatchi, L. O. Anderson, and Y. E. Shimabukuro: 2007, 'Spatial patterns and fire response of recent Amazonian droughts'. *Geophysical Research Letters* **34**(7), L07701.

Araújo, A. C., A. D. Nobre, B. Kruijt, J. A. Elbers, R. Dallarosa, P. Stefani, C. von Randow, A. O. Manzi, A. D. Culf, J. H. C. Gash, R. Valentini, and P. Kabat: 2002, 'Comparative measurements of carbon dioxide fluxes from two nearby towers in a central Amazonian rainforest: The Manaus LBA site'. *Journal of Geophysical Research* **107**(D20), 8090.

Araujo-Murakami, A., C. E. Doughty, D. B. Metcalfe, J. E. Silva-Espejo, L. Arroyo, J. P. Heredia, M. Flores, R. Sibler, L. M. Mendizabal, E. Pardo-Toledo, M. Vega, L. Moreno, V. D. Rojas-Landivar, K. Halladay, C. A. Girardin, T. J. Killeen, and Y. Malhi: 2014, 'The productivity, allocation and cycling of carbon in forests at the dry margin of the Amazon forest in Bolivia'. *Plant Ecology & Diversity* **7**(1-2), 55–69.

Baldocchi, D. D.: 2003, 'Assessing the eddy covariance technique for evaluating carbon dioxide exchange rates of ecosystems: Past, present and future'. *Global Change Biology* **9**(4), 479–492.

Baldocchi, D. D., E. Falge, L. Gu, R. Olson, D. Hollinger, S. Running, P. Anthoni, C. Bernhofer, K. Davis, R. Evans, J. Fuentes, A. Goldstein, G. Katul, B. Law, X. Lee, Y. Malhi, T. Meyers, W. Munger, W. Oechel, K. T. Paw, K. Pilegaard, H. P. Schmid, R. Valentini, S. Verma, T. Vesala, K. Wilson, and S. Wofsy: 2001, 'FLUXNET: A new tool to study the temporal and spatial variability of ecosystem-scale carbon dioxide, water vapor, and energy flux densities'. *Bulletin of the American Meteorological Society* **82**(11), 2415–2434.

Biudes, M. S., M. C. Souza, N. G. Machado, V. H. de Morais Danelichen, G. L. Vourlitis, and J. de Souza Nogueira: 2014, 'Modelling gross primary production of a tropical semi-deciduous forest in the southern Amazon Basin'. *International Journal of Remote Sensing* **35**(4), 1540–1562.

Brando, P. M., S. J. Goetz, A. Baccini, D. C. Nepstad, P. S. A. Beck, and M. C. Christman: 2010, 'Seasonal and interannual variability of climate and vegetation indices across the Amazon'. *Proceedings of the National Academy of Sciences of the United States of America* **107**(33), 14685–14690.

Brando, P. M., D. C. Nepstad, E. A. Davidson, S. E. Trumbore, D. Ray, and P. Camargo: 2008, 'Drought effects on litterfall, wood production and belowground carbon cycling in an Amazon forest: results of a throughfall reduction experiment'. *Philosophical transactions of the Royal Society of London. Series B, Biological sciences* **363**(1498), 1839–1848.

Bréon, F.-M., F. Maignan, M. Leroy, and I. Grant: 2002, 'Analysis of hot spot directional signatures measured from space'. *Journal of Geophysical Research* **107**(D16).

Caccamo, G., L. Chisholm, R. Bradstock, and M. Puotinen: 2011, 'Assessing the sensitivity of MODIS to monitor drought in high biomass ecosystems'. *Remote Sensing of Environment* **115**(10), 2626–2639.

Carswell, F. E., A. L. Costa, M. Palheta, Y. Malhi, P. Meir, J. d. P. R. Costa, M. d. L. Ruivo, L. d. S. M. Leal, J. M. N. Costa, R. J. Clement, and J. Grace: 2002, 'Seasonality in CO2 and H2O flux at an eastern Amazonian rain forest'. *Journal of Geophysical Research* **107**(D20), 8076.

Carvalho, L. M. V., C. Jones, A. N. D. Posadas, R. Quiroz, B. Bookhagen, and B. Liebmann: 2012, 'Precipitation characteristics of the South American Monsoon System derived from multiple datasets'. *Journal of Climate* **25**(13), 4600–4620.

Chen, B., N. C. Coops, D. Fu, H. A. Margolis, B. D. Amiro, T. A. Black, M. A. Arain, A. G. Barr, C. P.-A. Bourque, L. B. Flanagan, P. M. Lafleur, J. H. McCaughey, and S. C. Wofsy: 2012, 'Characterizing spatial representativeness of flux tower eddy-covariance measurements across the Canadian Carbon Program Network using remote sensing and footprint analysis'. *Remote Sensing of Environment* **124**, 742–755.

Chopping, M. J.: 2008, 'Terrestrial Applications of Multiangle Remote Sensing'. In: S. Liang (ed.): *9th International Symposium on Physical Measurements and Signatures in Remote Sensing*. Dordrecht, pp. 95–144, Springer.

Christensen, J. H., B. Hewitson, A. Busuioc, A. Chen, X. Gao, I. Held, R. Jones, R. K. Kolli, W.-T. Kwon, R. Laprise, V. M. Rueda, L. Mearns, C. G. Menéndez, J. Räisänen, A. Rinke, A. Sarr, and P. Whetton: 2007, 'Regional climate projections'. In: S. Solomon, D. Qin, M. Manning, Z. Chen, M. Marquis, K. Averyt, M. Tignor, and H. Miller (eds.): *Climate Change 2007: The Physical Science Basis. Contribution of Working Group I to the Fourth Assessment Report of the Intergovernmental Panel on Climate Change*. Cambridge, United Kingdom and New York, NY, USA: Cambridge University Press, Chapt. 11, pp. 847–940.

Christensen, J. H., K. K. Kanikicharla, E. Aldrian, S.-I. An, I. F. A. Cavalcanti, M. de Castro, W. Dong, P. Goswami, A. Hall, J. K. Kanyanga, A. Kitoh, J. Kossin, N.-C. Lau, J. Renwick, D. B. Stephenson, S.-P. Xie, and T. Zhou: 2013, 'Climate phenomena and their relevance for future regional climate change'. In: T. Stocker, D. Qin, G.-K. Plattner, M. Tignor, S. Allen, J. Boschung, A. Nauels, Y. Xia, V. Bex, and P. Midgley (eds.): *Climate Change 2013: The Physical Science Basis. Contribution of Working Group I to the Fifth Assessment Report of the Intergovernmental Panel on Climate Change*. Cambridge, United Kingdom and New York, NY, USA: Cambridge University Press, Chapt. 14, pp. 1217–1308.

Collins, M., S.-I. An, W. Cai, A. Ganachaud, E. Guilyardi, F.-F. Jin, M. Jochum, M. Lengaigne, S. Power, A. Timmermann, G. Vecchi, and A. Wittenberg: 2010, 'The impact of global warming on the tropical Pacific Ocean and El Niño'. *Nature Geoscience* **3**(6), 391–397.

Cox, P. M., R. A. Betts, M. Collins, P. P. Harris, C. Huntingford, and C. D. Jones: 2004, 'Amazonian forest dieback under climate-carbon cycle projections for the 21st century'. *Theoretical and Applied Climatology* **78**(1-3), 137–156.

Davis, K. J., P. S. Bakwin, C. Yi, B. W. Berger, C. Zhao, R. M. Teclaw, and J. G. Isebrands: 2003, 'The annual cycles of CO2 and H2O exchange over a northern mixed forest as observed from a very tall tower'. *Global Change Biology* **9**(9), 1278–1293.

de Abelleyra, D. and S. R. Verón: 2014, 'Comparison of different BRDF correction methods to generate daily normalized MODIS 250m time series'. *Remote Sensing of Environment* **140**, 46–59.

de Jong, R., S. de Bruin, A. de Wit, M. E. Schaepman, and D. L. Dent: 2011, 'Analysis of monotonic greening and browning trends from global NDVI time-series'. *Remote Sensing of Environment* **115**(2), 692–702.

de Toledo, J. J., W. E. Magnusson, and C. V. Castilho: 2013, 'Competition, exogenous disturbances and senescence shape tree size distribution in tropical forest: Evidence from tree mode of death in Central Amazonia'. *Journal of Vegetation Science* **24**(4), 651–663.

Doughty, C. E. and M. L. Goulden: 2008, 'Seasonal patterns of tropical forest leaf area index and CO2 exchange'. *Journal of Geophysical Research* **113**, G00B06.

Doughty, C. E., D. B. Metcalfe, M. C. da Costa, A. A. de Oliveira, G. F. Neto, J. A. Silva, L. E. Aragão, S. S. Almeida, C. A. Quesada, C. A. Girardin, K. Halladay, A. C. da Costa, and Y. Malhi: 2014, 'The production, allocation and cycling of carbon in a forest on fertile terra preta soil in eastern Amazonia compared with a forest on adjacent infertile soil'. *Plant Ecology & Diversity* **7**(1-2), 41–53.

Drolet, G. G., K. F. Huemmrich, F. G. Hall, E. M. Middleton, T. A. Black, A. G. Barr, and H. A. Margolis: 2005, 'A MODIS-derived photochemical reflectance index to detect inter-annual variations in the photosynthetic light-use efficiency of a boreal deciduous forest'. *Remote Sensing of Environment* **98**(2-3), 212–224.

Eltahir, E. A. B. and R. L. Bras: 1994, 'Precipitation recycling in the Amazon basin'. *Quarterly Journal of the Royal Meteorological Society* **120**(518), 861–880.

Friedl, M. A., D. Sulla-Menashe, B. Tan, A. Schneider, N. Ramankutty, A. Sibley, and X. Huang: 2010, 'MODIS collection 5 global land cover: Algorithm refinements and characterization of new datasets'. *Remote Sensing of Environment* **114**(1), 168–182.

Frolking, S., T. Milliman, M. Palace, D. Wisser, R. Lammers, and M. Fahnestock: 2011, 'Tropical forest backscatter anomaly evident in SeaWinds scatterometer morning overpass data during 2005 drought in Amazonia'. *Remote Sensing of Environment* **115**(3), 897–907.

Fu, R., L. Yin, W. Li, P. A. Arias, R. E. Dickinson, L. Huang, S. Chakraborty, K. Fernandes, B. Liebmann, R. Fisher, and R. B. Myneni: 2013, 'Increased dry-season length over southern Amazonia in recent decades and its implication for future climate projection'. *Proceedings of the National Academy of Sciences of the United States of America* **110**(45), 18110–18115.

Galvão, L. S., J. R. dos Santos, D. A. Roberts, F. M. Breunig, M. Toomey, and Y. M. de Moura: 2011, 'On intra-annual EVI variability in the dry season of tropical forest: A case study with MODIS and hyperspectral data'. *Remote Sensing of Environment* **115**(9), 2350–2359.

Gao, F., C. Schaaf, A. Strahler, Y. Jin, and X. Li: 2003, 'Detecting vegetation structure using a kernel-based BRDF model'. *Remote Sensing of Environment* **86**(2), 198–205.

Gao, X., A. R. Huete, W. Ni, and T. Miura: 2000, 'Optical-Biophysical Relationships of Vegetation Spectra without Background Contamination'. *Remote Sensing of Environment* **74**(3), 609–620.

Glenn, E. P., A. R. Huete, P. L. Nagler, and S. G. Nelson: 2008, 'Relationship between remotely-sensed vegetation indices, canopy attributes and plant physiological processes: What vegetation indices can and cannot tell us about the landscape'. *Sensors* **8**(4), 2136–2160.

Hashimoto, H., W. Wang, C. Milesi, M. A. White, S. Ganguly, M. Gamo, R. Hirata, R. B. Myneni, and R. R. Nemani: 2012, 'Exploring simple algorithms for estimating gross primary production in forested areas from satellite data'. *Remote Sensing* **4**(12), 303–326.

Hirota, M., C. Nobre, M. D. Oyama, and M. M. C. Bustamante: 2010, 'The climatic sensitivity of the forest, savanna and forest-savanna transition in tropical South America'. *The New Phytologist* **187**(3), 707–719.

Hu, B., W. Lucht, X. Li, and A. H. Strahler: 1997, 'Validation of kernel-driven semiempirical models for the surface bidirectional reflectance distribution function of land surfaces'. *Remote Sensing of Environment* **62**(3), 201–214.

Huete, A., K. Didan, T. Miura, E. Rodriguez, X. Gao, and L. Ferreira: 2002, 'Overview of the radiometric and biophysical performance of the MODIS vegetation indices'. *Remote Sensing of Environment* **83**(1-2), 195–213.

Huete, A., K. Didan, W. van Leeuwen, T. Miura, and E. Glenn: 2011, 'MODIS vegetation indices'. In: B. Ramachandran, C. O. Justice, and M. J. Abrams (eds.): *Land Remote Sensing and Global Environmental Change – NASA's Earth Observing System and the Science of ASTER and MODIS*. New York, Dordrecht, Heidelberg, London: Springer, Chapt. 26, pp. 579–602.

Huete, A. R., K. Didan, Y. E. Shimabukuro, P. Ratana, S. R. Saleska, L. R. Hutyra, W. Yang, R. R. Nemani, and R. Myneni: 2006, 'Amazon rainforests green-up with sunlight in dry season'. *Geophysical Research Letters* **33**(6), L06405.

Huffman, G. J., R. F. Adler, D. T. Bolvin, and E. J. Nelkin: 2010, 'The TRMM Multi-Satellite Precipitation Analysis (TMPA)'. In: M. Gebremichael and F. Hossain (eds.): *Satellite Rainfall Applications for Surface Hydrology*. Dordrecht: Springer Netherlands, pp. 3–22.

Hutyra, L. R., J. W. Munger, S. R. Saleska, E. Gottlieb, B. C. Daube, A. L. Dunn, D. F. Amaral, P. B. de Camargo, and S. C. Wofsy: 2007, 'Seasonal controls on the exchange of carbon and water in an Amazonian rain forest'. *Journal of Geophysical Research* **112**(G3), G03008.

Jiang, Z., A. Huete, K. Didan, and T. Miura: 2008, 'Development of a two-band enhanced vegetation index without a blue band'. *Remote Sensing of Environment* **112**(10), 3833–3845.

Jiao, Z., M. J. Hill, C. B. Schaaf, H. Zhang, Z. Wang, and X. Li: 2014, 'An Anisotropic Flat Index (AFX) to derive BRDF archetypes from MODIS'. *Remote Sensing of Environment* **141**, 168–187.

Kasischke, E. S., J. M. Melack, and M. C. Dobson: 1997, 'The use of imaging radars for ecological applications – A review'. *Remote Sensing of Environment* **59**(2), 141–156.

Kimes, D., W. Newcomb, R. Nelson, and J. Schutt: 1986, 'Directional reflectance distributions of a hardwood and pine forest canopy'. *IEEE Transactions on Geoscience and Remote Sensing* **GE-24**(2), 281–293.

Li, W., R. Fu, and R. E. Dickinson: 2006, 'Rainfall and its seasonality over the Amazon in the 21st century as assessed by the coupled models for the IPCC AR4'. *Journal of Geophysical Research* **111**(D2), D02111.

Li, W., R. Fu, R. I. N. Juárez, and K. Fernandes: 2008, 'Observed change of the standardized precipitation index, its potential cause and implications to future climate change in the Amazon region'. *Philosophical transactions of the Royal Society of London. Series B, Biological sciences* **363**(1498), 1767–72.

Liu, Y. Y., A. I. J. M. van Dijk, M. F. McCabe, J. P. Evans, and R. A. M. de Jeu: 2013, 'Global vegetation biomass change (1988-2008) and attribution to environmental and human drivers'. *Global Ecology and Biogeography* **22**(6), 692–705.

Lucht, W., C. Schaaf, and A. Strahler: 2000a, 'An algorithm for the retrieval of albedo from space using semiempirical BRDF models'. *IEEE Transactions on Geoscience and Remote Sensing* **38**(2), 977–998.

Lucht, W., C. B. Schaaf, A. H. Strahler, and R. P. D'Entremont: 2000b, 'Remote sensing of albedo using the BRDF in relation to land surface properties'. In: M. M. Verstraete, M. Menenti, and J. Peltoniemi (eds.): *Observing Land from Space: Science, Customers and Technology*. Dordrecht, Boston, London: Springer Netherlands, Chapt. 19, pp. 175–186.

Malhi, Y., F. Farfán Amézquita, C. E. Doughty, J. E. Silva-Espejo, C. A. Girardin, D. B. Metcalfe, L. E. Aragão, L. P. Huaraca-Quispe, I. Alzamora-Taype, L. Eguiluz-Mora, T. R. Marthews, K. Halladay, C. A. Quesada, A. L. Robertson, J. B. Fisher, J. Zaragoza-Castells, C. M. Rojas-Villagra, Y. Pelaez-Tapia, N. Salinas, P. Meir, and O. L. Phillips: 2014, 'The productivity, metabolism and carbon cycle of two lowland tropical forest plots in south-western Amazonia, Peru'. *Plant Ecology & Diversity* **7**(1-2), 85–105.

Malhi, Y., J. T. Roberts, R. A. Betts, T. J. Killeen, W. Li, and C. A. Nobre: 2008, 'Climate change, deforestation, and the fate of the Amazon'. *Science* **319**(5860), 169–172.

Malhi, Y., D. Wood, T. R. Baker, J. Wright, O. L. Phillips, T. Cochrane, P. Meir, J. Chave, S. Almeida, L. Arroyo, N. Higuchi, T. J. Killeen, S. G. Laurance, W. F. Laurance, S. L. Lewis, A. Monteagudo, D. A. Neill, P. Vargas, N. C. A. Nunez Pitman, C. Quesada, R. Alberto Salomao, J. N. M. Silva, A. T. Lezama, J. Terborgh, R. Martinez, and B. Vasquez Vinceti: 2006, 'The regional variation of aboveground live biomass in old-growth Amazonian forests'. *Global Change Biology* **12**(7), 1107–1138.

Marengo, J. A., B. Liebmann, V. E. Kousky, N. P. Filizola, and I. C. Wainer: 2001, 'Onset and end of the rainy season in the brazilian amazon basin'. *Journal of Climate* **14**(5), 833–852.

Marengo, J. A., C. A. Nobre, G. Sampaio, L. F. Salazar, and L. S. Borma: 2011, 'Climate change in the Amazon Basin: Tipping points, changes in extremes, and impacts on natural and human systems'. In: M. B. Bush, J. R. Flenley, and W. D. Gosling (eds.): *Tropical Rainforest Responses to Climatic Change*. Berlin, Heidelberg: Springer, Chapt. 9, pp. 259–283.

Markesteijn, L. and L. Poorter: 2009, 'Seedling root morphology and biomass allocation of 62 tropical tree species in relation to drought- and shade-tolerance'. *Journal of Ecology* **97**(2), 311–325.

Mayorga, E., M. Logsdon, M. Ballester, and J. Richey: 2012, 'BA-ECO CD-06 Amazon River Basin Land and Stream Drainage Direction Maps'. http://dx.doi.org/10.3334/ORNLDAAC/1086.

Mayorga, E., M. G. Logsdon, M. V. R. Ballester, and J. E. Richey: 2005, 'Estimating cell-to-cell land surface drainage paths from digital channel networks, with an application to the Amazon basin'. *Journal of Hydrology* **315**(1-4), 167–182.

McKee, T. B., N. J. Doesken, and J. Kleist: 1993, 'The relationship of drought frequency and duration to time scales'. In: *Eighth Conference on Applied Climatology, 17-22 January 1993*. Anaheim, California, pp. 17–22.

Meroni, M., M. Rossini, L. Guanter, L. Alonso, U. Rascher, R. Colombo, and J. Moreno: 2009, 'Remote sensing of solar-induced chlorophyll fluorescence: Review of methods and applications'. *Remote Sensing of Environment* **113**(10), 2037–2051.

Morton, D. C., J. Nagol, C. C. Carabajal, J. Rosette, M. Palace, B. D. Cook, E. F. Vermote, D. J. Harding, and P. R. J. North: 2014, 'Amazon forests maintain consistent canopy structure and greenness during the dry season'. *Nature* **506**, 221–224.

Moura, Y. M., L. S. Galvão, J. R. dos Santos, D. A. Roberts, and F. M. Breunig: 2012, 'Use of MISR/Terra data to study intra- and inter-annual EVI variations in the dry season of tropical forest'. *Remote Sensing of Environment* **127**, 260–270.

Myneni, R. B., W. Yang, R. R. Nemani, A. R. Huete, R. E. Dickinson, Y. Knyazikhin, K. Didan, R. Fu, R. I. Negrón Juárez, S. S. Saatchi, H. Hashimoto, K. Ichii, N. V. Shabanov, B. Tan, P. Ratana, J. L. Privette, J. T. Morisette, E. F. Vermote, D. P. Roy, R. E. Wolfe, M. A. Friedl, S. W. Running, P. Votava, N. El-Saleous, S. Devadiga, Y. Su, and V. V. Salomonson: 2007, 'Large seasonal swings in leaf area of Amazon rainforests'. *Proceedings of the National Academy of Sciences of the United States of America* **104**(12), 4820–4823.

Nemani, R. R., C. D. Keeling, H. Hashimoto, W. M. Jolly, S. C. Piper, C. J. Tucker, R. B. Myneni, and S. W. Running: 2003, 'Climate-driven increases in global terrestrial net primary production from 1982 to 1999'. *Science* **300**(5625), 1560–1563.

Nepstad, D. C., C. R. de Carvalho, E. A. Davidson, P. H. Jipp, P. A. Lefebvre, G. H. Negreiros, E. D. da Silva, T. A. Stone, S. E. Trumbore, and S. Vieira: 1994, 'The role of deep roots in the hydrological and carbon cycles of Amazonian forests and pastures'. *Nature* **372**(6507), 666–669.

Nepstad, D. C., P. Moutinho, M. B. Dias-Filho, E. Davidson, G. Cardinot, D. Markewitz, R. Figueiredo, N. Vianna, J. Chambers, D. Ray, J. B. Guerreiros, P. Lefebvre, L. Sternberg, M. Moreira, L. Barros, F. Y. Ishida, I. Tohlver, E. Belk, K. Kalif, and K. Schwalbe: 2002, 'The effects of partial throughfall exclusion on canopy processes, aboveground production, and biogeochemistry of an Amazon forest'. *Journal of Geophysical Research* **107**(D20), 8085.

Ouma, Y. O., T. Owiti, E. Kipkorir, J. Kibiiy, and R. Tateishi: 2012, 'Multitemporal comparative analysis of TRMM-3B42 satellite-estimated rainfall with surface gauge data at basin scales: daily, decadal and monthly evaluations'. *International Journal of Remote Sensing* **33**(24), 7662–7684.

Phillips, O. L., L. E. O. C. Aragão, S. L. Lewis, J. B. Fisher, J. Lloyd, G. López-González, Y. Malhi, A. Monteagudo, J. Peacock, C. A. Quesada, G. van der Heijden, S. Almeida, I. Amaral, L. Arroyo, G. Aymard, T. R. Baker, O. Bánki, L. Blanc, D. Bonal, P. Brando, J. Chave, A. C. A. de Oliveira, N. D. Cardozo, C. I. Czimczik, T. R. Feldpausch, M. A. Freitas, E. Gloor, N. Higuchi, E. Jiménez, G. Lloyd, P. Meir, C. Mendoza, A. Morel, D. A. Neill, D. Nepstad, S. Patiño, M. C. Peñuela, A. Prieto, F. Ramírez, M. Schwarz, J. Silva, M. Silveira, A. S. Thomas, H. T. Steege, J. Stropp, R. Vásquez, P. Zelazowski, E. Alvarez Dávila, S. Andelman, A. Andrade, K.-j. Chao, T. Erwin, A. Di Fiore, E. Honorio C, H. Keeling, T. J. Killeen, W. F. Laurance, A. Peña Cruz, N. C. A. Pitman, P. Núñez Vargas, H. Ramírez-Angulo, A. Rudas, R. Salamão, N. Silva, J. Terborgh, and A. Torres-Lezama: 2009, 'Drought sensitivity of the Amazon rainforest'. *Science* **323**(5919), 1344–1347.

Phillips, O. L., G. van der Heijden, S. L. Lewis, G. López-González, L. E. O. C. Aragão, J. Lloyd, Y. Malhi, A. Monteagudo, S. Almeida, E. A. Dávila, I. Amaral, S. Andelman, A. Andrade, L. Arroyo, G. Aymard, T. R. Baker, L. Blanc, D. Bonal, A. C. A. de Oliveira, K.-J. Chao, N. D. Cardozo, L. da Costa, T. R. Feldpausch, J. B. Fisher, N. M. Fyllas, M. A. Freitas, D. Galbraith, E. Gloor, N. Higuchi, E. Honorio, E. Jiménez, H. Keeling, T. J. Killeen, J. C. Lovett, P. Meir, C. Mendoza, A. Morel, P. N. n. Vargas, S. Patiño, K. S.-H. Peh, A. P. n. Cruz, A. Prieto, C. A. Quesada, F. Ramírez, H. Ramírez, A. Rudas, R. Salamão, M. Schwarz, J. Silva, M. Silveira, J. W. F. Slik, B. Sonké, A. S. Thomas, J. Stropp, J. R. D. Taplin, R. Vásquez, and E. Vilanova: 2010, 'Drought-mortality relationships for tropical forests'. *The New Phytologist* **187**(3), 631–646.

Poorter, L. and Y. Hayashida-Oliver: 2000, 'Effects of seasonal drought on gap and understorey seedlings in a Bolivian moist forest'. *Journal of Tropical Ecology* **16**(4), 481–498.

Rahman, A. F., D. A. Sims, V. D. Cordova, and B. Z. El-Masri: 2005, 'Potential of MODIS EVI and surface temperature for directly estimating per-pixel ecosystem C fluxes'. *Geophysical Research Letters* **32**(19), L19404.

Raich, J. W., E. B. Rastetter, J. M. Melillo, D. W. Kicklighter, P. A. Steudler, B. J. Peterson, A. L. Grace, B. M. III, and C. J. Vorosmarty: 1991, 'Potential net primary productivity in south america: Application of a global model'. *Ecological Applications* **1**(4), 399.

Rammig, A., T. Jupp, K. Thonicke, B. Tietjen, J. Heinke, S. Ostberg, W. Lucht, W. Cramer, and P. Cox: 2010, 'Estimating the risk of Amazonian forest dieback'. *The New Phytologist* **187**(3), 694–706.

Roberts, D. A., B. W. Nelson, J. B. Adams, and F. Palmer: 1998, 'Spectral changes with leaf aging in Amazon caatinga'. *Trees* **12**(6), 315–325.

Roujean, J.-L., M. Leroy, and P.-Y. Deschamps: 1992, 'A bidirectional reflectance model of the Earth's surface for the correction of remote sensing data'. *Journal of Geophysical Research* **97**(D18), 20455.

Running, S. W., R. R. Nemani, F. A. Heinsch, M. Zhao, M. Reeves, and H. Hashimoto: 2004, 'A continuous satellite-derived measure of global terrestrial primary production'. *BioScience* **54**(6), 547.

Saatchi, S., S. Asefi-Najafabady, Y. Malhi, L. E. O. C. Aragão, L. O. Anderson, R. B. Myneni, and R. Nemani: 2013, 'Persistent effects of a severe drought on Amazonian forest canopy'. *Proceedings of the National Academy of Sciences of the United States of America* **110**(2), 565–570.

Saleska, S. R., K. Didan, A. R. Huete, and H. R. da Rocha: 2007, 'Amazon forests green-up during 2005 drought'. *Science* **318**(5850), 612.

Saleska, S. R., S. D. Miller, D. M. Matross, M. L. Goulden, S. C. Wofsy, H. R. da Rocha, P. B. de Camargo, P. Crill, B. C. Daube, H. C. de Freitas, L. Hutyra, M. Keller, V. Kirchhoff, M. Menton, J. W. Munger, E. H. Pyle, A. H. Rice, and H. Silva: 2003, 'Carbon in Amazon forests: unexpected seasonal fluxes and disturbance-induced losses'. *Science* **302**(5650), 1554–1557.

Samanta, A., S. Ganguly, H. Hashimoto, S. Devadiga, E. Vermote, Y. Knyazikhin, R. R. Nemani, and R. B. Myneni: 2010, 'Amazon forests did not green-up during the 2005 drought'. *Geophysical Research Letters* **37**(5), L05401.

Samanta, A., S. Ganguly, E. Vermote, R. R. Nemani, and R. B. Myneni: 2012a, 'Interpretation of variations in MODIS-measured greenness levels of Amazon forests during 2000 to 2009'. *Environmental Research Letters* **7**(2), 024018.

Samanta, A., S. Ganguly, E. Vermote, R. R. Nemani, and R. B. Myneni: 2012b, 'Why is remote sensing of Amazon forest greenness so challenging?'. *Earth Interactions* **16**(7), 1–14.

Samanta, A., Y. Knyazikhin, L. Xu, R. E. Dickinson, R. Fu, M. H. Costa, S. S. Saatchi, R. R. Nemani, and R. B. Myneni: 2012c, 'Seasonal changes in leaf area of Amazon forests from leaf flushing and abscission'. *Journal of Geophysical Research* **117**(G1), G01015.

Schaaf, C. B., F. Gao, A. H. Strahler, W. Lucht, X. Li, T. Tsang, N. C. Strugnell, X. Zhang, Y. Jin, J.-P. Muller, P. Lewis, M. Barnsley, P. Hobson, M. Disney, G. Roberts, M. Dunderdale, C. Doll, R. P. D'Entremont, B. Hu, S. Liang, J. L. Privette, and D. Roy: 2002, 'First operational BRDF, albedo nadir reflectance products from MODIS'. *Remote Sensing of Environment* **83**(1-2), 135–148.

Schaaf, C. B., J. Liu, F. Gao, and A. H. Strahler: 2011, 'Aqua and Terra MODIS albedo and reflectance anisotropy products'. In: B. Ramachandran, C. O. Justice, and M. J. Abrams (eds.): *Land Remote Sensing and Global Environmental Change – NASA's Earth Observing System and the Science of ASTER and MODIS*. New York, Dordrecht, Heidelberg, London: Springer, Chapt. 23, pp. 579–602.

Schwalm, C. R., C. A. Williams, K. Schaefer, A. Arneth, D. Bonal, N. Buchmann, J. Chen, B. E. Law, A. Lindroth, S. Luyssaert, M. Reichstein, and A. D. Richardson: 2010, 'Assimilation exceeds respiration sensitivity to drought: A FLUXNET synthesis'. *Global Change Biology* **16**(2), 657–670.

Sharma, R. C., K. Kajiwara, and Y. Honda: 2013, 'Estimation of forest canopy structural parameters using kernel-driven bi-directional reflectance model based multi-angular vegetation indices'. *ISPRS Journal of Photogrammetry and Remote Sensing* **78**, 50–57.

Silva, F. B., Y. E. Shimabukuro, L. E. O. C. Aragão, L. O. Anderson, G. Pereira, F. Cardozo, and E. Arai: 2013, 'Large-scale heterogeneity of Amazonian phenology revealed from 26-year long AVHRR/NDVI time-series'. *Environmental Research Letters* **8**(2), 024011.

Sims, D. A., A. F. Rahman, V. D. Cordova, B. Z. El-Masri, D. D. Baldocchi, L. B. Flanagan, A. H. Goldstein, D. Y. Hollinger, L. Misson, R. K. Monson, W. C. Oechel, H. P. Schmid, S. C. Wofsy, and L. Xu: 2006, 'On the use of MODIS EVI to assess gross primary productivity of North American ecosystems'. *Journal of Geophysical Research* **111**(G4), G04015.

Sims, D. A., A. F. Rahman, E. F. Vermote, and Z. Jiang: 2011, 'Seasonal and inter-annual variation in view angle effects on MODIS vegetation indices at three forest sites'. *Remote Sensing of Environment* **115**(12), 3112–3120.

Sitch, S., C. Huntingford, N. Gedney, P. E. Levy, M. Lomas, S. L. Piao, R. Betts, P. Ciais, P. Cox, P. Friedlingstein, C. D. Jones, I. C. Prentice, and F. I. Woodward: 2008, 'Evaluation of the terrestrial carbon cycle, future plant geography and climate-carbon cycle feedbacks using five Dynamic Global Vegetation Models (DGVMs)'. *Global Change Biology* **14**(9), 2015–2039.

Soares-Filho, B. S., D. C. Nepstad, L. M. Curran, G. C. Cerqueira, R. A. Garcia, C. A. Ramos, E. Voll, A. McDonald, P. Lefebvre, and P. Schlesinger: 2006, 'Modelling conservation in the Amazon basin'. *Nature* **440**(7083), 520–523.

Strahler, A. H., J.-P. Muller, and MODIS Science Team Members: 1999, 'MODIS BRDF/Albedo Product: Algorithm theoretical basis document version 5.0'. http://modis.gsfc.nasa.gov/data/atbd/atbd_mod09.pdf.

Tan, B., C. Woodcock, J. Hu, P. Zhang, M. Ozdogan, D. Huang, W. Yang, Y. Knyazikhin, and R. Myneni: 2006, 'The impact of gridding artifacts on the local spatial properties of MODIS data: Implications for validation, compositing, and band-to-band registration across resolutions'. *Remote Sensing of Environment* **105**(2), 98–114.

Toomey, M., D. Roberts, and B. Nelson: 2009, 'The influence of epiphylls on remote sensing of humid forests'. *Remote Sensing of Environment* **113**(8), 1787–1798.

Trenberth, K. E., A. Dai, G. van der Schrier, P. D. Jones, J. Barichivich, K. R. Briffa, and J. Sheffield: 2013, 'Global warming and changes in drought'. *Nature Climate Change* **4**(1), 17–22.

Turner, D. P., W. D. Ritts, W. B. Cohen, S. T. Gower, S. W. Running, M. Zhao, M. H. Costa, A. a. Kirschbaum, J. M. Ham, S. R. Saleska, and D. E. Ahl: 2006, 'Evaluation of MODIS NPP and GPP products across multiple biomes'. *Remote Sensing of Environment* **102**(3-4), 282–292.

Vermote, E., C. Justice, and F.-M. Breon: 2009, 'Towards a Generalized Approach for Correction of the BRDF Effect in MODIS Directional Reflectances'. *IEEE Transactions on Geoscience and Remote Sensing* **47**(3), 898–908.

von Randow, C., L. D. A. Sá, P. S. S. D. Gannabathula, A. O. Manzi, P. R. A. Arlino, and B. Kruijt: 2002, 'Scale variability of atmospheric surface layer fluxes of energy and carbon over a tropical rain forest in southwest Amazonia 1. Diurnal conditions'. *Journal of Geophysical Research* **107**(D20), 8062.

Wang, D., D. Morton, J. Masek, A. Wu, J. Nagol, X. Xiong, R. Levy, E. Vermote, and R. Wolfe: 2012, 'Impact of sensor degradation on the MODIS NDVI time series'. *Remote Sensing of Environment* **119**, 55–61.

White, A., M. Cannell, and A. Friend: 1999, 'Climate change impacts on ecosystems and the terrestrial carbon sink: A new assessment'. *Global Environmental Change* **9**, S21–S30.

WMO/UNESCO: 2011, 'International glossary of hydrology'. http://webworld.unesco.org/water/ihp/db/glossary/glu/EN/GF0372EN.HTM.

Xiao, X., S. Hagen, Q. Zhang, M. Keller, and B. Moore: 2006, 'Detecting leaf phenology of seasonally moist tropical forests in South America with multi-temporal MODIS images'. *Remote Sensing of Environment* **103**(4), 465–473.

Xiao, X., D. Hollinger, J. Aber, M. Goltz, E. A. Davidson, Q. Zhang, and B. Moore: 2004a, 'Satellite-based modeling of gross primary production in an evergreen needleleaf forest'. *Remote Sensing of Environment* **89**(4), 519–534.

Xiao, X., Q. Zhang, B. Braswell, S. Urbanski, S. Boles, S. Wofsy, B. Moore, and D. Ojima: 2004b, 'Modeling gross primary production of temperate deciduous broadleaf forest using satellite images and climate data'. *Remote Sensing of Environment* **91**(2), 256–270.

Xiao, X., Q. Zhang, S. Saleska, L. Hutyra, P. De Camargo, S. Wofsy, S. Frolking, S. Boles, M. Keller, and B. Moore: 2005, 'Satellite-based modeling of gross primary production in a seasonally moist tropical evergreen forest'. *Remote Sensing of Environment* **94**(1), 105–122.

Xu, L., A. Samanta, M. H. Costa, S. Ganguly, R. R. Nemani, and R. B. Myneni: 2011, 'Widespread decline in greenness of Amazonian vegetation due to the 2010 drought'. *Geophysical Research Letters* **38**(7), L07402.

Zhao, M. and S. W. Running: 2010, 'Drought-induced reduction in global terrestrial net primary production from 2000 through 2009'. *Science* **329**(5994), 940–943.

Appendix

This Appendix offers additional graphs parallel to the approaches presented in this report. They closely follow the same processing of the referenced methods and differing details are described. All graphs are referrered to in the text.

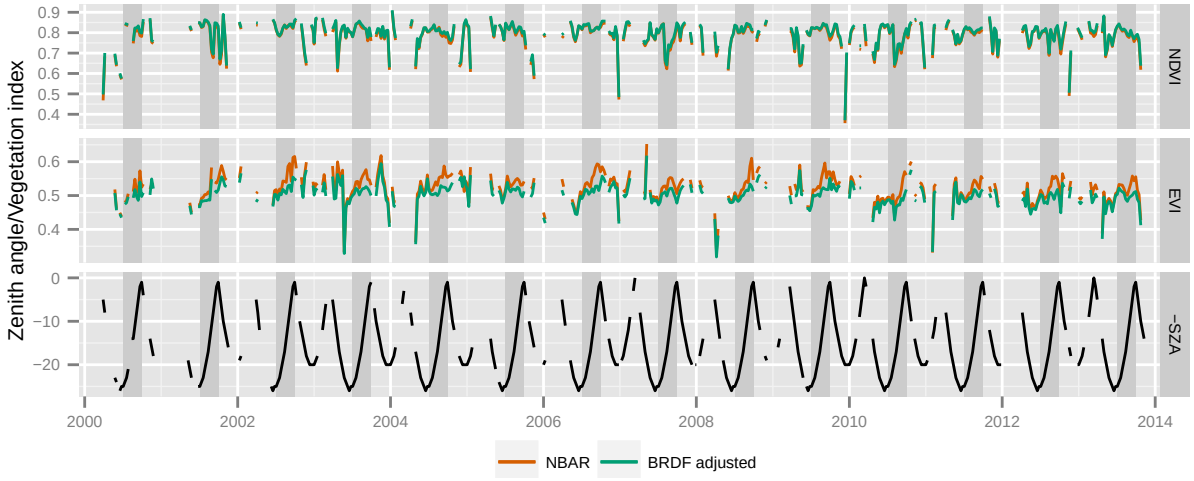

Figure A.1: Same as Figure 4.3, but based on 3 × 3 km window around BR-Ma2 (see Figure 3.1)

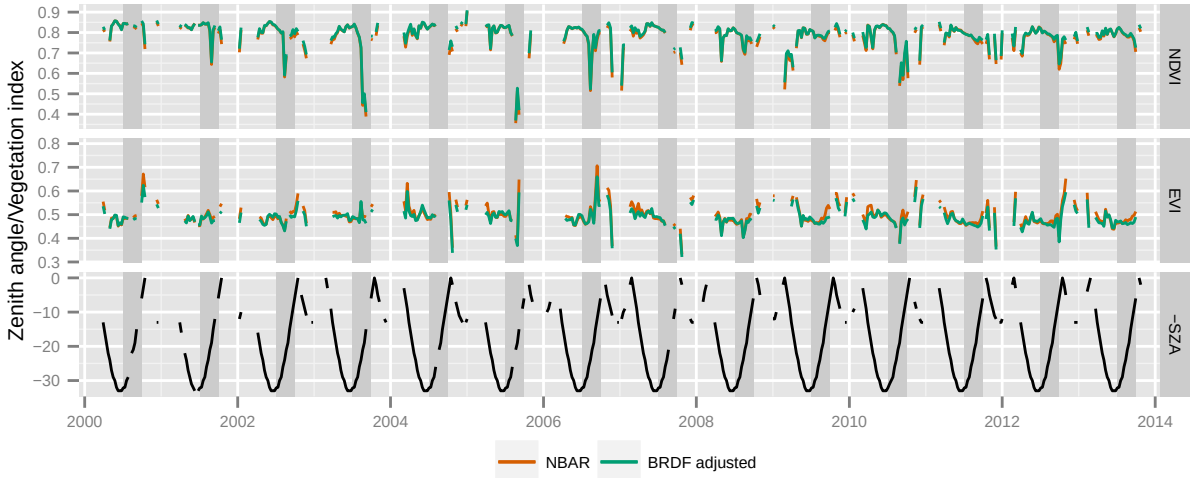

Figure A.2: Same as Figure 4.3, but based on 3 × 3 km window around BR-Ji2 (see Figure 3.1)

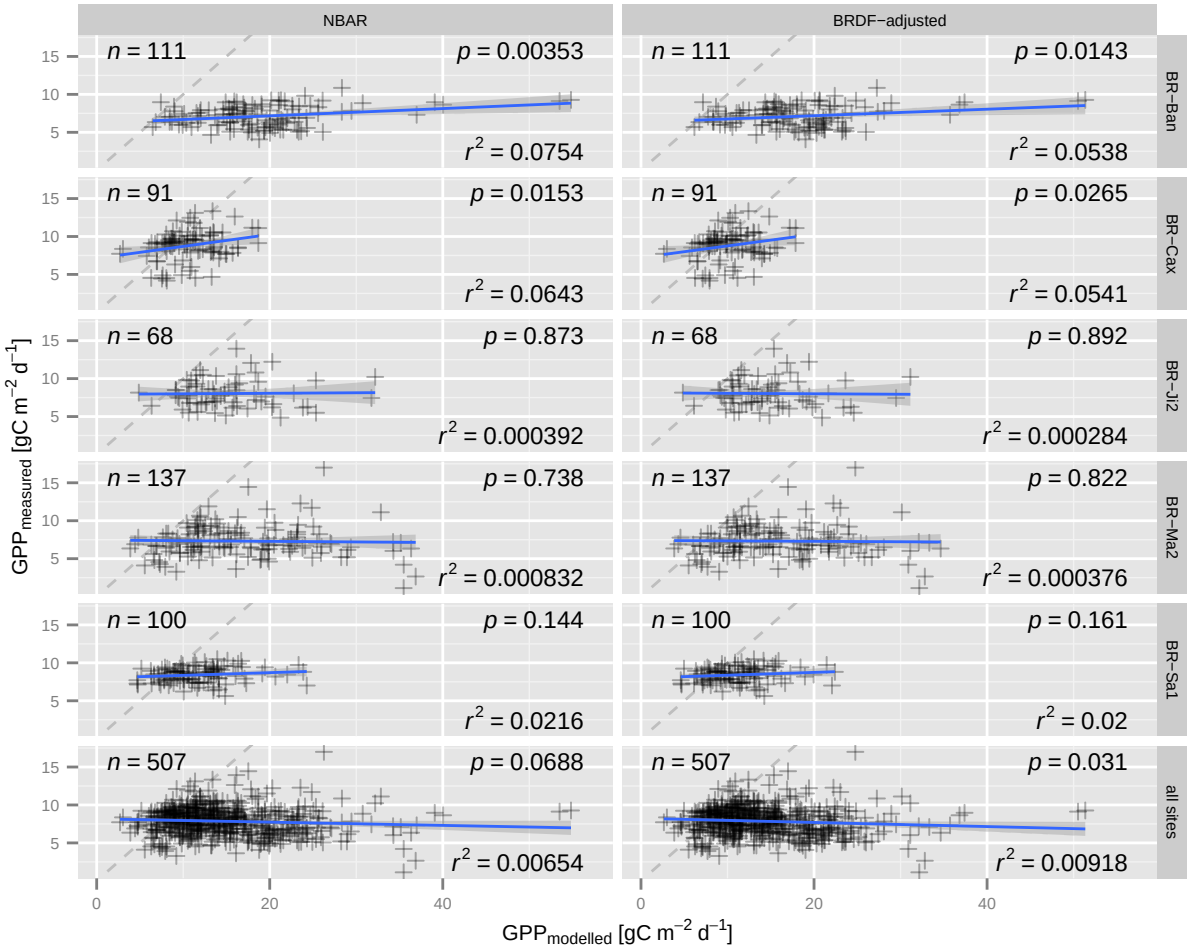

Figure A.3: Same as Figure 4.5, but using the VPM formulation of Biudes et al. (2014)

As mentioned in Section 3.4, Biudes et al. (2014) proposed a modification of the VPM to model Gross Primary Productivity (GPP) for semi-seasonal tropical forests. They empirically derived an alternative formulation for the water scalar (Eq. 3.8), which was based on the Photosynthetic Photon Flux Density (PPFD) and relative humidity as predictors for the water scalar in a statistical model. Since the model formulation using PPFD as the only predictor of the water scalar was performing almost as good as the PPFD and relative humidity combined model, I used the simpler first one. The water scalar W_{scalar} is given as:

$$W_{scalar} = \exp^{0.0035 \cdot (PPFD - 325.30)} \tag{A.1}$$

As Figure A.3 shows, the modified model strongly overestimated GPP at all sites. Biudes et al. (2014) statistically fitted the VPM to a semi-seasonal fluxtower site (Sinop-Mato Grosso, BR-Mtg), which might be the reason for this poor performance.

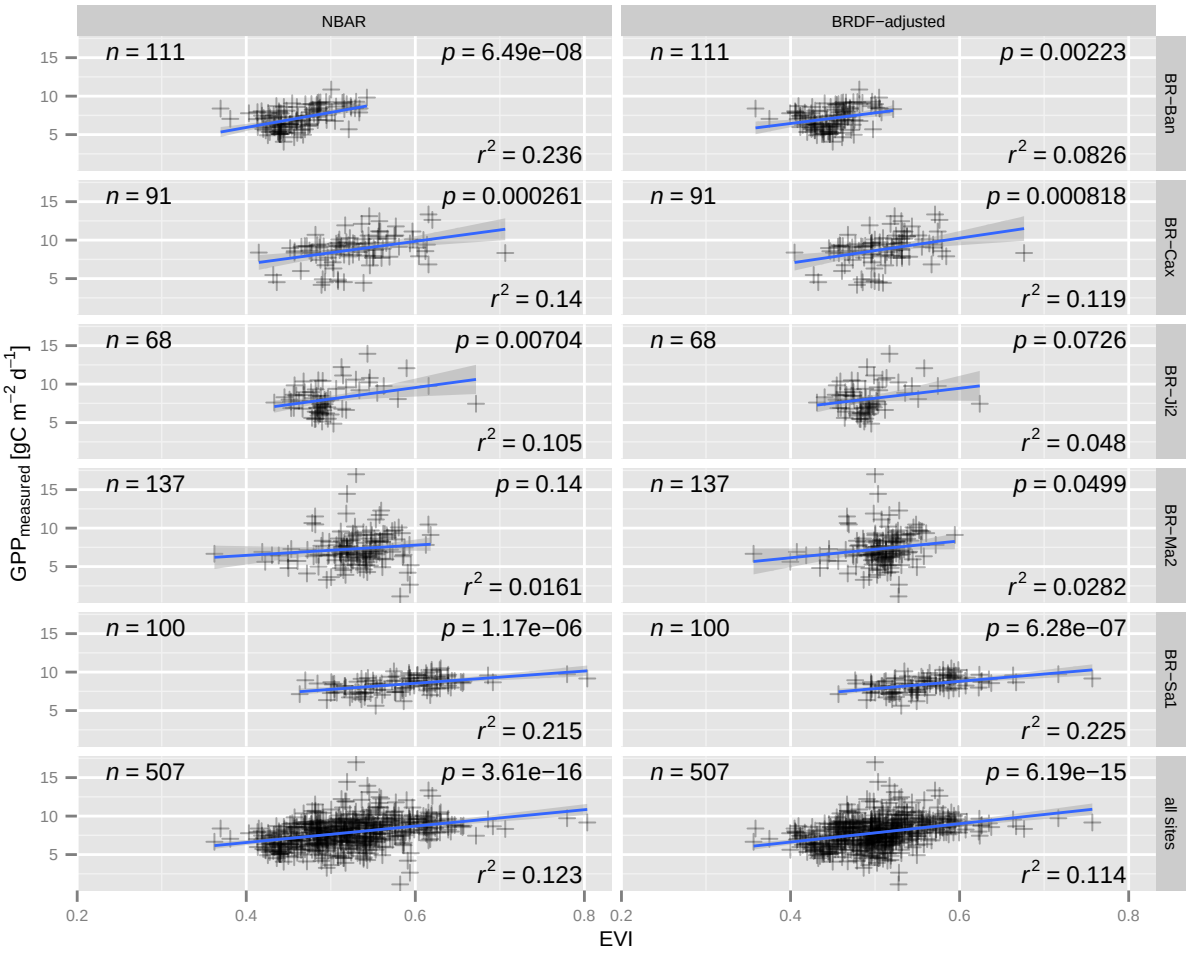

Figure A.4: Same as Figure 4.5, but directly using EVI as prediction of GPP